

Shearlets and Optimally Sparse Approximations

Gitta Kutyniok, Jakob Lemvig, and Wang-Q Lim

Abstract Multivariate functions are typically governed by anisotropic features such as edges in images or shock fronts in solutions of transport-dominated equations. One major goal both for the purpose of compression as well as for an efficient analysis is the provision of optimally sparse approximations of such functions. Recently, cartoon-like images were introduced in 2D and 3D as a suitable model class, and approximation properties were measured by considering the decay rate of the L^2 error of the best N -term approximation. Shearlet systems are to date the only representation system, which provide optimally sparse approximations of this model class in 2D as well as 3D. Even more, in contrast to all other directional representation systems, a theory for compactly supported shearlet frames was derived which moreover also satisfy this optimality benchmark. This chapter shall serve as an introduction to and a survey about sparse approximations of cartoon-like images by band-limited and also compactly supported shearlet frames as well as a reference for the state-of-the-art of this research field.

1 Introduction

Scientists face a rapidly growing deluge of data, which requires highly sophisticated methodologies for analysis and compression. Simultaneously, the complexity of the

Gitta Kutyniok

Institute of Mathematics, University of Osnabrück, 49069 Osnabrück, Germany, e-mail: kutyniok@math.uni-osnabrueck.de

Jakob Lemvig

Institute of Mathematics, University of Osnabrück, 49069 Osnabrück, Germany, e-mail: jlemvig@math.uni-osnabrueck.de

Wang-Q Lim

Institute of Mathematics, University of Osnabrück, 49069 Osnabrück, Germany, e-mail: wlim@math.uni-osnabrueck.de

data is increasing, evidenced in particular by the observation that data becomes increasingly high-dimensional. One of the most prominent features of data are singularities which is justified, for instance, by the observation from computer visionists that the human eye is most sensitive to smooth geometric areas divided by sharp edges. Intriguingly, already the step from univariate to multivariate data causes a significant change in the behavior of singularities. Whereas one-dimensional (1D) functions can only exhibit point singularities, singularities of two-dimensional (2D) functions can already be of both point as well as curvilinear type. Thus, in contrast to *isotropic* features – point singularities –, suddenly *anisotropic* features – curvilinear singularities – are possible. And, in fact, multivariate functions are typically governed by *anisotropic phenomena*. Think, for instance, of edges in digital images or evolving shock fronts in solutions of transport-dominated equations. These two exemplary situations also show that such phenomena occur even for both explicitly as well as implicitly given data.

One major goal both for the purpose of compression as well as for an efficient analysis is the introduction of representation systems for ‘good’ approximation of anisotropic phenomena, more precisely, of multivariate functions governed by anisotropic features. This raises the following fundamental questions:

- (P1) What is a suitable model for functions governed by anisotropic features?
- (P2) How do we measure ‘good’ approximation and what is a benchmark for optimality?
- (P3) Is the step from 1D to 2D already the crucial step or how does this framework scale with increasing dimension?
- (P4) Which representation system behaves optimally?

Let us now first debate these questions on a higher and more intuitive level, and later on delve into the precise mathematical formalism.

1.1 Choice of Model for Anisotropic Features

Each model design has to face the trade-off between closeness to the true situation versus sufficient simplicity to enable analysis of the model. The suggestion of a suitable model for functions governed by anisotropic features in [9] solved this problem in the following way. As a model for an image, it first of all requires the $L^2(\mathbb{R}^2)$ functions serving as a model to be supported on the unit square $[0, 1]^2$. These functions shall then consist of the minimal number of smooth parts, namely two. To avoid artificial problems with a discontinuity ending at the boundary of $[0, 1]^2$, the boundary curve of one of the smooth parts is entirely contained in $(0, 1)^2$. It now remains to decide upon the regularity of the smooth parts of the model functions and of the boundary curve, which were chosen to both be C^2 . Thus, concluding, a possible suitable model for functions governed by anisotropic features are 2D functions which are supported on $[0, 1]^2$ and C^2 apart from a closed C^2 discontinuity curve; these are typically referred to as *cartoon-like images* (cf. chapter [1]). This provides

an answer to (P1). Extensions of this 2D model to piecewise smooth curves were then suggested in [4], and extensions to 3D as well as to different types of regularity were introduced in [11, 15].

1.2 Measure for Sparse Approximation and Optimality

The quality of the performance of a representation system with respect to cartoon-like images is typically measured by taking a non-linear approximation viewpoint. More precisely, given a cartoon-like image and a representation system which forms an orthonormal basis, the chosen measure is the asymptotic behavior of the L^2 error of the best N -term (non-linear) approximation in the number of terms N . This intuitively measures how fast the ℓ^2 norm of the tail of the expansion decays as more and more terms are used for the approximation. A slight subtlety has to be observed if the representation system does not form an orthonormal basis, but a frame. In this case, the N -term approximation using the N largest coefficients is considered which, in case of an orthonormal basis, is the same as the best N -term approximation, but not in general. The term ‘optimally sparse approximation’ is then awarded to those representation systems which deliver the fastest possible decay rate in N for all cartoon-like images, where we consider log-factors as negligible, thereby providing an answer to (P2).

1.3 Why is 3D the Crucial Dimension?

We already identified the step from 1D to 2D as crucial for the appearance of anisotropic features at all. Hence one might ask: Is it sufficient to consider only the 2D situation, and higher dimensions can be treated similarly? Or: Does each dimension causes its own problems? To answer these questions, let us consider the step from 2D to 3D which shows a curious phenomenon. A 3D function can exhibit point (= 0D), curvilinear (= 1D), and surface (= 2D) singularities. Thus, suddenly anisotropic features appear in two different dimensions: As one-dimensional and as two-dimensional features. Hence, the 3D situation has to be analyzed with particular care. It is not at all clear whether two different representation systems are required for optimally approximating both types of anisotropic features simultaneously, or whether one system will suffice. This shows that the step from 2D to 3D can justifiably be also coined ‘crucial’. Once it is known how to handle anisotropic features of different dimensions, the step from 3D to 4D can be dealt with in a similar way as also the extension to even higher dimensions. Thus, answering (P3), we conclude that the two crucial dimensions are 2D and 3D with higher dimensional situations deriving from the analysis of those.

1.4 Performance of Shearlets and Other Directional Systems

Within the framework we just briefly outlined, it can be shown that wavelets do not provide optimally sparse approximations of cartoon-like images. This initiated a flurry of activity within the applied harmonic analysis community with the aim to develop so-called *directional* representation systems which satisfy this benchmark, certainly besides other desirable properties depending in the application at hand. In 2004, Candés and Donoho were the first to introduce with the tight curvelet frames a directional representation system which provides provably optimally sparse approximations of cartoon-like images in the sense we discussed. One year later, contourlets were introduced by Do and Vetterli [7], which similarly derived an optimal approximation rate. The first analysis of the performance of (band-limited) shearlet frames was undertaken by Guo and Labate in [10], who proved that these shearlets also do satisfy this benchmark. In the situation of (band-limited) shearlets the analysis was then driven even further, and very recently Guo and Labate proved a similar result for 3D cartoon-like images which in this case are defined as a function which is C^2 apart from a C^2 discontinuity surface, i.e., focusing on only one of the types of anisotropic features we are facing in 3D.

1.5 Band-Limited Versus Compactly Supported Systems

The results mentioned in the previous subsection only concerned band-limited systems. Even in the contourlet case, although compactly supported contourlets seem to be included, the proof for optimal sparsity only works for band-limited generators due to the requirement of infinite directional vanishing moments. However, for various applications compactly supported generators are inevitable, wherefore already in the wavelet case the introduction of compactly supported wavelets was a major advance. Prominent examples of such applications are imaging sciences, when an image might need to be denoised while avoiding a smoothing of the edges, or in the theory of partial differential equations as a generating system for a trial space in order to ensure fast computational realizations.

So far, shearlets are the only system, for which a theory for compactly supported generators has been developed and compactly supported shearlet frames have been constructed [13], see also the survey paper [16]. It should though be mentioned that these frames are somehow close to being tight, but at this point it is not clear whether also compactly supported *tight* shearlet frames can be constructed. Interestingly, it was proved in [17] that this class of shearlet frames also delivers optimally sparse approximations of the 2D cartoon-like image model class with a very different proof than [10] now adapted to the particular nature of compactly supported generators. And with [15] the 3D situation is now also fully understood, even taking the two different types of anisotropic features – curvilinear and surface singularities – into account.

1.6 Outline

In Sect. 2, we introduce the 2D and 3D cartoon-like image model class. Optimality of sparse approximations of this class are then discussed in Sect. 3. Sect. 4 is concerned with the introduction of 3D shearlet systems with both band-limited and compactly supported generators, which are shown to provide optimally sparse approximations within this class in the final Sect. 5.

2 Cartoon-like Image Class

We start by making the in the introduction of this chapter already intuitively derived definition of cartoon-like images mathematically precise. We start with the most basic definition of this class which was also historically first stated in [9]. We allow ourselves to state this together with its 3D version from [11] by remarking that d could be either $d = 2$ or $d = 3$.

For fixed $\mu > 0$, the class $\mathcal{E}^2(\mathbb{R}^d)$ of *cartoon-like image* shall be the set of functions $f : \mathbb{R}^d \rightarrow \mathbb{C}$ of the form

$$f = f_0 + f_1 \chi_B,$$

where $B \subset [0, 1]^d$ and $f_i \in C^2(\mathbb{R}^d)$ with $\text{supp } f_0 \subset [0, 1]^d$ and $\|f_i\|_{C^2} \leq \mu$ for each $i = 0, 1$. For dimension $d = 2$, we assume that ∂B is a closed C^2 -curve with curvature bounded by ν , and, for $d = 3$, the discontinuity ∂B shall be a closed C^2 -surface with principal curvatures bounded by ν . An indiscriminately chosen cartoon-like function $f = \chi_B$, where the discontinuity surface ∂B is a deformed sphere in \mathbb{R}^3 , is depicted in Fig. 1.

Since ‘objects’ in images often have sharp corners, in [4] for 2D and in [15] for 3D also less regular images were allowed, where ∂B is only assumed to be *piecewise* C^2 -smooth. We note that this viewpoint is also essential for being able to analyze the behavior of a system with respect to the two different types of anisotropic features appearing in 3D; see the discussion in Subsection 1.3. Letting $L \in \mathbb{N}$ denote the number of C^2 pieces, we speak of the extended class of *cartoon-like images* $\mathcal{E}_L^2(\mathbb{R}^d)$ as consisting of cartoon-like images having C^2 -smoothness apart from a piecewise C^2 discontinuity curve in the 2D setting and a piecewise C^2 discontinuity surface in the 3D setting. Indeed, in the 3D setting, besides the C^2 discontinuity surfaces, this model exhibits curvilinear C^2 singularities as well as point singularities, e.g., the cartoon-like image $f = \chi_B$ in Fig. 2 exhibits a discontinuity surface $\partial B \subset \mathbb{R}^3$ consisting of *three* C^2 -smooth surfaces with point and curvilinear singularities where these surfaces meet.

The model in [15] goes even one step further and considers a different regularity for the smooth parts, say being in C^β , and for the smooth pieces of the discontinuity, say being in C^α with $1 \leq \alpha \leq \beta \leq 2$. This very general class of cartoon-like images is then denoted by $\mathcal{E}_{\alpha,L}^\beta(\mathbb{R}^d)$, with the agreement that $\mathcal{E}_L^2(\mathbb{R}^d) = \mathcal{E}_{\alpha,L}^\beta(\mathbb{R}^d)$ for $\alpha = \beta = 2$.

Fig. 1 A simple cartoon-like image $f = \chi_B \in \mathcal{C}_L^2(\mathbb{R}^3)$ with $L = 1$ for dimension $d = 3$, where the discontinuity surface ∂B is a deformed sphere.

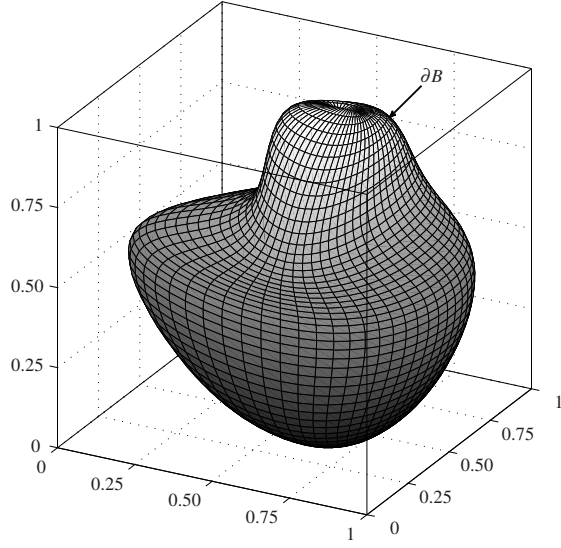
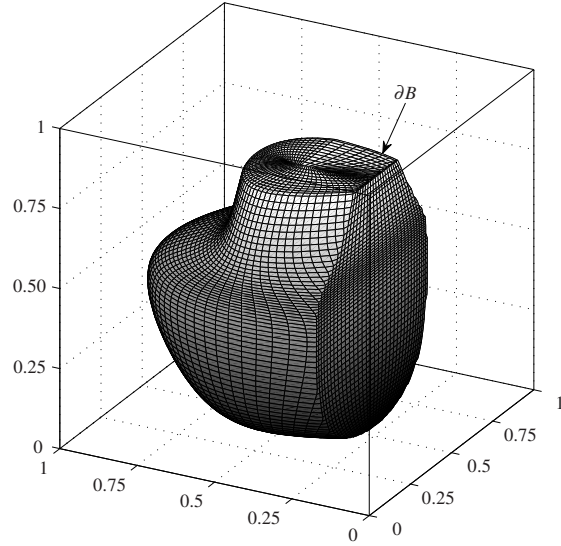


Fig. 2 A cartoon-like image $f = \chi_B \in \mathcal{C}_L^2(\mathbb{R}^3)$ with $L = 3$, where the discontinuity surface ∂B is piecewise C^2 smooth.



For the purpose of clarity, in the sequel we will focus on the first most basic cartoon-like model where $\alpha = \beta = 2$, and add hints on generalizations when appropriate (in particular, in Sect. 5.2.4).

3 Sparse Approximations

After having clarified the model situation, we will now discuss which measure for the accuracy of approximation by representation systems we choose, and what optimality means in this case.

3.1 (Non-Linear) N -term Approximations

Let \mathcal{C} denote a given class of elements in a separable Hilbert space \mathcal{H} with norm $\|\cdot\| = \langle \cdot, \cdot \rangle^{1/2}$ and $\Phi = (\phi_i)_{i \in I}$ a dictionary for \mathcal{H} , i.e., $\overline{\text{span}} \Phi = \mathcal{H}$, with indexing set I . The dictionary Φ plays the role of our representation system. Later \mathcal{C} will be chosen to be the class of cartoon-like images and Φ a shearlet frame, but for now we will assume this more general setting. We now seek to approximate each single element of \mathcal{C} with elements from Φ by ‘few’ terms of this system. Approximation theory provides us with the concept of best N -term approximation which we now introduce; for a general introduction to approximation theory, we refer to [6].

For this, let $f \in \mathcal{C}$ be arbitrarily chosen. Since Φ is a complete system, for any $\varepsilon > 0$ there exists a finite linear combination of elements from Φ of the form

$$g = \sum_{i \in F} c_i \phi_i \quad \text{with } F \subset I \text{ finite, i.e., } \#|F| < \infty$$

such that $\|f - g\| \leq \varepsilon$. Moreover, if Φ is a frame with countable indexing set I , there exists a sequence $(c_i)_{i \in I} \in \ell_2(I)$ such that the representation

$$f = \sum_{i \in I} c_i \phi_i$$

holds with convergence in the Hilbert space norm $\|\cdot\|$. The reader should notice that, if Φ does not form a basis, this representation of f is certainly not the only possible one. Letting now $N \in \mathbb{N}$, we aim to approximate f by only N terms of Φ , i.e., by

$$\sum_{i \in I_N} c_i \phi_i \quad \text{with } I_N \subset I, \#|I_N| = N,$$

which is termed *N -term approximation* to f . This approximation is typically *non-linear* in the sense that if f_N is an N -term approximation to f with indices I_N and g_N is an N -term approximation to some $g \in \mathcal{C}$ with indices J_N , then $f_N + g_N$ is only an N -term approximation to $f + g$ in case $I_N = J_N$.

But certainly we would like to pick the ‘best’ approximation with the accuracy of approximation measured in the Hilbert space norm. We define the *best N -term approximation* to f by the N -term approximation

$$f_N = \sum_{i \in I_N} c_i \phi_i,$$

which satisfies that, for all $I_N \subset I$, $\#|I_N| = N$, and for all scalars $(c_i)_{i \in I}$,

$$\|f - f_N\| \leq \left\| f - \sum_{i \in I_N} c_i \phi_i \right\|.$$

Let us next discuss the notion of best N -term approximation for the special cases of Φ forming an orthonormal basis, a tight frame, and a general frame alongside an error estimate for the accuracy of this approximation.

3.1.1 Orthonormal Bases

Let Φ be an orthonormal basis for \mathcal{H} . In this case, we can actually write down the best N -term approximation $f_N = \sum_{i \in I_N} c_i \phi_i$ for f . Since in this case

$$f = \sum_{i \in I} \langle f, \phi_i \rangle \phi_i,$$

and this representation is unique, we obtain

$$\begin{aligned} \|f - f_N\|_{\mathcal{H}} &= \left\| \sum_{i \in I} \langle f, \phi_i \rangle \phi_i - \sum_{i \in I_N} c_i \phi_i \right\| \\ &= \left\| \sum_{i \in I_N} [\langle f, \phi_i \rangle - c_i] \phi_i + \sum_{i \in I \setminus I_N} \langle f, \phi_i \rangle \phi_i \right\| \\ &= \|(\langle f, \phi_i \rangle - c_i)_{i \in I_N}\|_{\ell^2} + \|(\langle f, \phi_i \rangle)_{i \in I \setminus I_N}\|_{\ell^2}. \end{aligned}$$

The first term $\|(\langle f, \phi_i \rangle - c_i)_{i \in I_N}\|_{\ell^2}$ can be minimized by choosing $c_i = \langle f, \phi_i \rangle$ for all $i \in I_N$. And the second term $\|(\langle f, \phi_i \rangle)_{i \in I \setminus I_N}\|_{\ell^2}$ can be minimized by choosing I_N to be the indices of the N largest coefficients $\langle f, \phi_i \rangle$ in magnitude. Notice that this does not uniquely determine f_N since some coefficients $\langle f, \phi_i \rangle$ might have the same magnitude. But it characterizes the set of best N -term approximations to some $f \in \mathcal{C}$ precisely. Even more, we have complete control of the error of best N -term approximation by

$$\|f - f_N\| = \|(\langle f, \phi_i \rangle)_{i \in I \setminus I_N}\|_{\ell^2}. \quad (1)$$

3.1.2 Tight Frames

Assume now that Φ constitutes a tight frame with bound $A = 1$ for \mathcal{H} . In this situation, we still have

$$f = \sum_{i \in I} \langle f, \phi_i \rangle \phi_i,$$

but this expansion is now not unique anymore. Moreover, the frame elements are not orthogonal. Both conditions prohibit an analysis of the error of best N -term approximation as in the previously considered situation of an orthonormal basis. And

in fact, examples can be provided to show that selecting the N largest coefficients $\langle f, \phi_i \rangle$ in magnitude does not always lead to the *best* N -term approximation, but merely to an N -term approximation. To be able to still analyze the approximation error, one typically – as will be also our choice in the sequel – chooses the N -term approximation provided by the indices I_N associated with the N largest coefficients $\langle f, \phi_i \rangle$ in magnitude with these coefficients, i.e.,

$$f_N = \sum_{i \in I_N} \langle f, \phi_i \rangle \phi_i.$$

This selection also allows for some control of the approximation in the Hilbert space norm, which we will defer to the next subsection in which we consider the more general case of arbitrary frames.

3.1.3 General Frames

Let now Φ form a frame for \mathcal{H} with frame bounds A and B , and let $(\tilde{\phi}_i)_{i \in I}$ denote the canonical dual frame. We then consider the expansion of f in terms of this dual frame, i.e.,

$$f = \sum_{i \in I} \langle f, \phi_i \rangle \tilde{\phi}_i. \quad (2)$$

Notice that we could also consider

$$f = \sum_{i \in I} \langle f, \tilde{\phi}_i \rangle \phi_i.$$

Let us explain, why the first form is of more interest to us in this chapter. By definition, we have $(\langle f, \tilde{\phi}_i \rangle)_{i \in I} \in \ell^2(I)$ as well as $(\langle f, \phi_i \rangle)_{i \in I} \in \ell^2(I)$. Since we only consider expansions of functions f belonging to a subset \mathcal{C} of \mathcal{H} , this can, at least, potentially improve the decay rate of the coefficients so that they belong to $\ell^p(I)$ for some $p < 2$. This is exactly what is understood by *sparse approximation* (also called *compressible approximations* in the context of inverse problems). We hence aim to analyze shearlets with respect to this behavior, i.e., the decay rate of shearlet coefficients. This then naturally leads to form (2). We remark that in case of a tight frame, there is no distinction necessary, since then $\tilde{\phi}_i = \phi_i$ for all $i \in I$.

As in the tight frame case, it is not possible to derive a usable, explicit form for the best N -term approximation. We therefore again crudely approximate the best N -term approximation by choosing the N -term approximation provided by the indices I_N associated with the N largest coefficients $\langle f, \phi_i \rangle$ in magnitude with these coefficients, i.e.,

$$f_N = \sum_{i \in I_N} \langle f, \phi_i \rangle \tilde{\phi}_i.$$

But, surprisingly, even with this rather crude greedy selection procedure, we obtain very strong results for the approximation rate of shearlets as we will see in Sect. 5.

The following result shows how the N -term approximation error can be bounded by the tail of the square of the coefficients c_i . The reader might want to compare this result with the error in case of an orthonormal basis stated in (1).

Lemma 1. *Let $(\phi_i)_{i \in I}$ be a frame for \mathcal{H} with frame bounds A and B , and let $(\tilde{\phi}_i)_{i \in I}$ be the canonical dual frame. Let $I_N \subset I$ with $\#I_N = N$, and let f_N be the N -term approximation $f_N = \sum_{i \in I_N} \langle f, \phi_i \rangle \tilde{\phi}_i$. Then*

$$\|f - f_N\|^2 \leq \frac{1}{A} \sum_{i \notin I_N} |\langle f, \phi_i \rangle|^2. \quad (3)$$

Proof. Recall that the canonical dual frame satisfies the frame inequality with bounds B^{-1} and A^{-1} . At first hand, it therefore might look as if the estimate (3) should follow directly from the frame inequality for the canonical dual. However, since the sum in (3) does not run over the entire index set $i \in I$, but only $I \setminus I_N$, this is not the case. So, to prove the lemma, we first consider

$$\begin{aligned} \|f - f_N\| &= \sup \{ |\langle f - f_N, g \rangle| : g \in \mathcal{H}, \|g\| = 1 \} \\ &= \sup \left\{ \left| \sum_{i \notin I_N} \langle f, \phi_i \rangle \langle \tilde{\phi}_i, g \rangle \right| : g \in \mathcal{H}, \|g\| = 1 \right\}. \end{aligned} \quad (4)$$

Using Cauchy-Schwarz' inequality, we then have that

$$\left| \sum_{i \notin I_N} \langle f, \phi_i \rangle \langle \tilde{\phi}_i, g \rangle \right|^2 \leq \sum_{i \notin I_N} |\langle f, \phi_i \rangle|^2 \sum_{i \notin I_N} |\langle \tilde{\phi}_i, g \rangle|^2 \leq A^{-1} \|g\|^2 \sum_{i \notin I_N} |\langle f, \phi_i \rangle|^2,$$

where we have used the upper frame inequality for the dual frame $(\tilde{\phi}_i)_i$ in the second step. We can now continue (4) and arrive at

$$\|f - f_N\|^2 \leq \sup \left\{ \frac{1}{A} \|g\|^2 \sum_{i \notin I_N} |\langle f, \phi_i \rangle|^2 : g \in \mathcal{H}, \|g\| = 1 \right\} = \frac{1}{A} \sum_{i \notin I_N} |\langle f, \phi_i \rangle|^2.$$

□

Relating to the previous discussion about the decay of coefficients $\langle f, \phi_i \rangle$, let c^* denote the non-increasing (in modulus) rearrangement of $c = (c_i)_{i \in I} = (\langle f, \phi_i \rangle)_{i \in I}$, e.g., c_n^* denotes the n th largest coefficient of c in modulus. This rearrangement corresponds to a bijection $\pi : \mathbb{N} \rightarrow I$ that satisfies

$$\pi : \mathbb{N} \rightarrow I, \quad c_{\pi(n)} = c_n^* \text{ for all } n \in \mathbb{N}.$$

Strictly speaking, the rearrangement (and hence the mapping π) might not be unique; we will simply take c^* to be one of these rearrangements. Since $c \in \ell^2(I)$, also $c^* \in \ell^2(\mathbb{N})$. Suppose further that $|c_n^*|$ even decays as

$$|c_n^*| \lesssim n^{-(\alpha+1)/2} \quad \text{for } n \rightarrow \infty$$

for some $\alpha > 0$, where the notation $h(n) \lesssim g(n)$ means that there exists a $C > 0$ such that $h(n) \leq Cg(n)$, i.e., $h(n) = O(g(n))$. Clearly, we then have $c^* \in \ell^p(\mathbb{N})$ for $p \geq \frac{2}{\alpha+1}$. By Lemma 1, the N -term approximation error will therefore decay as

$$\|f - f_N\|^2 \leq \frac{1}{A} \sum_{n>N} |c_n^*|^2 \lesssim \sum_{n>N} n^{-\alpha+1} \asymp N^{-\alpha},$$

where f_N is the N -term approximation of f by keeping the N largest coefficients, that is,

$$f_N = \sum_{n=1}^N c_n^* \tilde{\phi}_{\pi(n)}. \quad (5)$$

The notation $h(n) \asymp g(n)$, also written $h(n) = \Theta(g(n))$, used above means that h is bounded both above and below by g asymptotically as $n \rightarrow \infty$, that is, $h(n) = O(g(n))$ and $g(n) = O(h(n))$.

3.2 A Notion of Optimality

We now return to the setting of functions spaces $\mathcal{H} = L^2(\mathbb{R}^d)$, where the subset \mathcal{C} will be the class of cartoon-like images, that is, $\mathcal{C} = \mathcal{E}_L^2(\mathbb{R}^d)$. We then aim for a benchmark, i.e., an optimality statement, for sparse approximation of functions in $\mathcal{E}_L^2(\mathbb{R}^d)$. For this, we will again only require that our representation system Φ is a dictionary, that is, we assume only that $\Phi = (\phi_i)_{i \in I}$ is a complete family of functions in $L^2(\mathbb{R}^d)$ with I not necessarily being countable. Without loss of generality, we can assume that the elements ϕ_i are normalized, i.e., $\|\phi_i\|_{L^2} = 1$ for all $i \in I$. For $f \in \mathcal{E}_L^2(\mathbb{R}^d)$ we then consider expansions of the form

$$f = \sum_{i \in I_f} c_i \phi_i,$$

where $I_f \subset I$ is a countable selection from I that may depend on f . Relating to the previous subsection, the first N elements of $\Phi_f := \{\phi_i\}_{i \in I_f}$ could for instance be the N terms from Φ selected for the best N -term approximation of f .

Since artificial cases shall be avoided, this selection procedure has the following natural restriction which is usually termed *polynomial depth search*: The n th term in Φ_f is obtained by only searching through the first $q(n)$ elements of the list Φ_f , where q is a polynomial. Moreover, the selection rule may *adaptively* depend on f , and the n th element may also be modified adaptively and depend on the first $(n-1)$ th chosen elements. We shall denote any sequence of coefficients c_i chosen according to these restrictions by $c(f) = (c_i)_i$. The role of the polynomial q is to limit how deep or how far down in the listed dictionary Φ_f we are allowed to search for the next element ϕ_i in the approximation. Without such a depth search limit, one could choose Φ to be a countable, dense subset of $L^2(\mathbb{R}^d)$ which would yield arbitrarily good sparse approximations, but also infeasible approximations in practise.

Using information theoretic arguments, it was then shown in [8, 15], that almost no matter what selection procedure we use to find the coefficients $c(f)$, we cannot have $\|c(f)\|_{\ell^p}$ bounded for $p < \frac{2(d-1)}{d+1}$ for $d = 2, 3$.

Theorem 1 ([8, 15]). *Retaining the definitions and notations in this subsection and allowing only polynomial depth search, we obtain*

$$\max_{f \in \mathcal{E}_L^2(\mathbb{R}^d)} \|c(f)\|_{\ell^p} = +\infty, \quad \text{for } p < \frac{2(d-1)}{d+1}.$$

In case Φ is an orthonormal basis for $L^2(\mathbb{R}^d)$, the norm $\|c(f)\|_{\ell^p}$ is trivially bounded for $p \geq 2$ since we can take $c(f) = (c_i)_{i \in I} = (\langle f, \phi_i \rangle)_{i \in I}$. Although not explicitly stated, the proof can be straightforwardly extended from 3D to higher dimensions as also the definition of cartoon-like images can be similarly extended. It is then intriguing to analyze the behavior of $\frac{2(d-1)}{d+1}$ from Thm. 1. In fact, as $d \rightarrow \infty$, we observe that $\frac{2(d-1)}{d+1} \rightarrow 2$. Thus, the decay of any $c(f)$ for cartoon-like images becomes slower as d grows and approaches ℓ^2 , which – as we just mentioned – is actually the rate guaranteed for *all* $f \in L^2(\mathbb{R}^d)$.

Thm. 1 is truly a statement about the optimal achievable sparsity level: No representation system – up to the restrictions described above – can deliver approximations for $\mathcal{E}_L^2(\mathbb{R}^d)$ with coefficients satisfying $c(f) \in \ell_p$ for $p < \frac{2(d-1)}{d+1}$. This implies the following lower bound

$$c(f)_n^* \gtrsim n^{-\frac{d+1}{2(d-1)}} = \begin{cases} n^{-3/2} & : d = 2, \\ n^{-1} & : d = 3. \end{cases} \quad (6)$$

where $c(f)^* = (c(f)_n^*)_{n \in \mathbb{N}}$ is a decreasing (in modulus) arrangement of the coefficients $c(f)$.

One might ask how this relates to the approximation error of (best) N -term approximation discussed before. For simplicity, suppose for a moment that Φ is actually an orthonormal basis (or more generally a Riesz basis) for $L^2(\mathbb{R}^d)$ with $d = 2$ and $d = 3$. Then – as discussed in Sect. 3.1.1 – the *best* N -term approximation to $f \in \mathcal{E}_L^2(\mathbb{R}^d)$ is obtained by keeping the N largest coefficients. Using the error estimate (1) as well as (6), we obtain

$$\|f - f_N\|_{L^2}^2 = \sum_{n > N} |c(f)_n^*|^2 \gtrsim \sum_{n > N} n^{-\frac{d+1}{d-1}} \asymp N^{-\frac{2}{d-1}},$$

i.e., the best N -term approximation error $\|f - f_N\|_{L^2}^2$ behaves asymptotically as $N^{-\frac{2}{d-1}}$ or worse. If, more generally, Φ is a frame, and f_N is chosen as in (5), we can similarly conclude that the asymptotic lower bound for $\|f - f_N\|_{L^2}^2$ is $N^{-\frac{2}{d-1}}$, that is, the optimally achievable rate is, at best, $N^{-\frac{2}{d-1}}$. Thus, this optimal rate can be used as a benchmark for measuring the sparse approximation ability of cartoon-like images of different representation systems. Let us phrase this formally.

Definition 1. Let $\Phi = (\phi_i)_{i \in I}$ be a frame for $L^2(\mathbb{R}^d)$ with $d = 2$ or $d = 3$. We say that Φ *provides optimally sparse approximations* of cartoon-like images if, for each $f \in \mathcal{E}_L^2(\mathbb{R}^d)$, the associated N -term approximation f_N (cf. (5)) by keeping the N largest coefficients of $c = c(f) = (\langle f, \phi_i \rangle)_{i \in I}$ satisfies

$$\|f - f_N\|_{L^2}^2 \lesssim N^{-\frac{2}{d-1}} \quad \text{as } N \rightarrow \infty, \quad (7)$$

and

$$|c_n^*| \lesssim n^{-\frac{d+1}{2(d-1)}} \quad \text{as } n \rightarrow \infty, \quad (8)$$

where we ignore log-factors.

Note that, for frames Φ , the bound $|c_n^*| \lesssim n^{-\frac{d+1}{2(d-1)}}$ automatically implies that $\|f - f_N\|^2 \lesssim N^{-\frac{2}{d-1}}$ whenever f_N is chosen as in (5). This follows from Lemma 1 and the estimate

$$\sum_{n>N} |c_n^*|^2 \lesssim \sum_{n>N} n^{-\frac{d+1}{d-1}} \lesssim \int_N^\infty x^{-\frac{d+1}{d-1}} dx \leq C \cdot N^{-\frac{2}{d-1}}, \quad (9)$$

where we have used that $-\frac{d+1}{d-1} + 1 = -\frac{2}{d-1}$. Hence, we are searching for a representation system Φ which forms a frame and delivers decay of $c = (\langle f, \phi_i \rangle)_{i \in I}$ as (up to log-factors)

$$|c_n^*| \lesssim n^{-\frac{d+1}{2(d-1)}} = \begin{cases} n^{-3/2} & : \quad d = 2, \\ n^{-1} & : \quad d = 3. \end{cases} \quad (10)$$

as $n \rightarrow \infty$ for any cartoon-like image.

3.3 Approximation by Fourier Series and Wavelets

We will next study two examples of more traditional representation systems – the Fourier basis and wavelets – with respect to their ability to meet this benchmark. For this, we choose the function $f = \chi_B$, where B is a ball contained in $[0, 1]^d$, again $d = 2$ or $d = 3$, as a simple cartoon-like image in $\mathcal{E}_L^2(\mathbb{R}^d)$ with $L = 1$, analyze the error $\|f - f_N\|^2$ for f_N being the N -term approximation by the N largest coefficients and compare with the optimal decay rate stated in Definition 1. It will however turn out that these systems are far from providing optimally sparse approximations of cartoon-like images, thus underlining the pressing need to introduce representation systems delivering this optimal rate; and we already now refer to Sect. 5 in which shearlets will be proven to satisfy this property.

Since Fourier series and wavelet systems are orthonormal bases (or more generally, Riesz bases) the best N -term approximation is found by keeping the N largest coefficients as discussed in Sect. 3.1.1.

3.3.1 Fourier Series

The error of the best N -term Fourier series approximation of a typical cartoon-like image decays asymptotically as $N^{-1/d}$. The following proposition shows this behavior in the case of a very simple cartoon-like image: The characteristic function on a ball.

Proposition 1. *Let $d \in \mathbb{N}$, and let $\Phi = (e^{2\pi i k x})_{k \in \mathbb{Z}^d}$. Suppose $f = \chi_B$, where B is a ball contained in $[0, 1]^d$. Then*

$$\|f - f_N\|_{L^2}^2 \asymp N^{-1/d} \quad \text{for } N \rightarrow \infty,$$

where f_N is the best N -term approximation from Φ .

Proof. We fix a new origin as the center of the ball B . Then f is a radial function $f(x) = h(\|x\|_2)$ for $x \in \mathbb{R}^d$. The Fourier transform of f is also a radial function and can be expressed explicitly by Bessel functions of first kind [14, 18]:

$$\hat{f}(\xi) = r^{d/2} \frac{J_{d/2}(2\pi r \|\xi\|_2)}{\|\xi\|_2^{d/2}},$$

where r is the radius of the ball B . Since the Bessel function $J_{d/2}(x)$ decays like $x^{-1/2}$ as $x \rightarrow \infty$, the Fourier transform of f decays like $|\hat{f}(\xi)| \asymp \|\xi\|_2^{-(d+1)/2}$ as $\|\xi\|_2 \rightarrow \infty$. Letting $I_N = \{k \in \mathbb{Z}^d : \|k\|_2 \leq N\}$ and f_N be the partial Fourier sum with terms from I_N , we obtain

$$\begin{aligned} \|f - f_N\|_{L^2}^2 &= \sum_{k \notin I_N} |\hat{f}(k)|^2 \asymp \int_{\|\xi\|_2 > N} \|\xi\|_2^{-(d+1)} d\xi \\ &= \int_N^\infty r^{-(d+1)} r^{(d-1)} dr = \int_N^\infty r^{-2} dr = N^{-1}. \end{aligned}$$

The conclusion now follows from the cardinality of $\#|I_N| \asymp N^d$ as $N \rightarrow \infty$. \square

3.3.2 Wavelets

Since wavelets are designed to deliver sparse representations of singularities – see Chapter [1] – we expect this system to outperform the Fourier approach. This will indeed be the case. However, the optimal rate will still by far be missed. The best N -term approximation of a typical cartoon-like image using a wavelet basis performs

only slightly better than Fourier series with asymptotic behavior as $N^{-1/(d-1)}$. This is illustrated by the following result.

Proposition 2. *Let $d = 2, 3$, and let Φ be a wavelet basis for $L^2(\mathbb{R}^d)$ or $L^2([0, 1]^d)$. Suppose $f = \chi_B$, where B is a ball contained in $[0, 1]^d$. Then*

$$\|f - f_n\|_{L^2}^2 \asymp N^{-\frac{1}{d-1}} \quad \text{for } N \rightarrow \infty,$$

where f_n is the best N -term approximation from Φ .

Proof. Let us first consider wavelet approximation by the Haar tensor wavelet basis for $L^2([0, 1]^d)$ of the form

$$\{\phi_{0,k} : |k| \leq 2^J - 1\} \cup \{\psi_{j,k}^1, \dots, \psi_{j,k}^{2^{d-1}} : j \geq J, |k| \leq 2^{j-J} - 1\},$$

where $J \in \mathbb{N}$, $k \in \mathbb{N}_0^d$, and $g_{j,k} = 2^{jd/2}g(2^j \cdot -k)$ for $g \in L^2(\mathbb{R}^d)$. There are only a finite number of coefficients of the form $\langle f, \phi_{0,k} \rangle$, hence we do not need to consider these for our asymptotic estimate. For simplicity, we take $J = 0$. At scale $j \geq 0$ there exist $\Theta(2^{j(d-1)})$ non-zero wavelet coefficients, since the surface area of ∂B is finite and the wavelet elements are of size $2^{-j} \times \dots \times 2^{-j}$.

To illustrate the calculations leading to the sought approximation error rate, we will first consider the case where B is a cube in $[0, 1]^d$. For this, we first consider the non-zero coefficients associated with the face of the cube containing the point (b, c, \dots, c) . For scale j , let k be such that $\text{supp } \psi_{j,k}^1 \cap \text{supp } f \neq \emptyset$, where $\psi^1(x) = h(x_1)p(x_2) \dots p(x_d)$ and h and p are the Haar wavelet and scaling function, respectively. Assume that b is located in the first half of the interval $[2^{-j}k_1, 2^{-j}(k_1 + 1)]$; the other case can be handled similarly. Then

$$|\langle f, \psi_{j,k}^1 \rangle| = \int_{2^{-j}k_1}^b 2^{jd/2} dx_1 \prod_{i=2}^d \int_{2^{-j}k_i}^{2^{-j}(k_i+1)} dx_i = (b - 2^{-j}k_1) 2^{-j(d-1)} 2^{jd/2} \asymp 2^{-jd/2},$$

where we have used that $(b - 2^{-j}k_1)$ will typically be of size $\frac{1}{4} 2^{-j}$. Note that for the chosen j and k above, we also have that $\langle f, \psi_{j,k}^l \rangle = 0$ for all $l = 2, \dots, 2^d - 1$.

There will be $2 \cdot \lceil 2c2^{j(d-1)} \rceil$ nonzero coefficients of size $2^{-jd/2}$ associated with the wavelet ψ^1 at scale j . The same conclusion holds for the other wavelets ψ^l , $l = 2, \dots, 2^d - 1$. To summarize, at scale j there will be $C2^{j(d-1)}$ nonzero coefficients of size $C2^{-jd/2}$. On the first j_0 scales, that is $j = 0, 1, \dots, j_0$, we therefore have $\sum_{j=0}^{j_0} 2^{j(d-1)} \asymp 2^{j_0(d-1)}$ nonzero coefficients. The n th largest coefficient c_n^* is of size $n^{-\frac{d}{2(d-1)}}$ since, for $n = 2^{j(d-1)}$, we have

$$2^{-j\frac{d}{2}} = n^{-\frac{d}{2(d-1)}}.$$

Therefore,

$$\|f - f_N\|_{L^2}^2 = \sum_{n>N} |c_n^*|^2 \asymp \sum_{n>N} n^{-\frac{d}{d-1}} \asymp \int_N^\infty x^{-\frac{d}{d-1}} dx = \frac{d}{d-1} N^{-\frac{1}{d-1}}.$$

Hence, for the best N -term approximation f_N of f using a wavelet basis, we obtain the asymptotic estimates

$$\|f - f_N\|_{L^2}^2 = \Theta(N^{-\frac{1}{d-1}}) = \begin{cases} \Theta(N^{-1}), & \text{if } d = 2, \\ \Theta(N^{-1/2}), & \text{if } d = 3, \end{cases}.$$

Let us now consider the situation that B is a ball. In fact, in this case we can do similar (but less transparent) calculations leading to the same asymptotic estimates as above. We will not repeat these calculations here, but simply remark that the upper asymptotic bound in $|\langle f, \psi_{j,k}^l \rangle| \asymp 2^{-jd/2}$ can be seen by the following general argument:

$$|\langle f, \psi_{j,k}^l \rangle| \leq \|f\|_{L^\infty} \|\psi_{j,k}^l\|_{L^1} \leq \|f\|_{L^\infty} \|\psi^l\|_{L^1} 2^{-jd/2} \leq C 2^{-jd/2},$$

which holds for each $l = 1, \dots, 2^d - 1$.

Finally, we can conclude from our calculations that choosing another wavelet basis will not improve the approximation rate. \square

Remark 1. We end this subsection with a remark on *linear* approximations. For a linear wavelet approximation of f one would use

$$f \approx \langle f, \phi_{0,0} \rangle \phi_{0,0} + \sum_{l=1}^{2^d-1} \sum_{j=0}^{j_0} \sum_{|k| \leq 2^j-1} \langle f, \psi_{j,k}^l \rangle \psi_{j,k}^l$$

for some $j_0 > 0$. If restricting to linear approximations, the summation order is not allowed to be changed, and we therefore need to include all coefficients from the first j_0 scales. At scale $j \geq 0$, there exist a total of 2^{jd} coefficients, which by our previous considerations can be bounded by $C \cdot 2^{-jd/2}$. Hence, we include 2^j times as many coefficients as in the non-linear approximation on each scale. This implies that the error rate of the linear N -term wavelet approximation is $N^{-1/d}$, which is the *same* rate as obtained by Fourier approximations.

3.3.3 Key Problem

The key problem of the suboptimal behavior of Fourier series and wavelet bases is the fact that these systems are not generated by anisotropic elements. Let us illustrate this for 2D in the case of wavelets. Wavelet elements are isotropic due to the scaling matrix $\text{diag}(2^j, 2^j)$. However, already intuitively, approximating a curve with isotropic elements requires many more elements than if the analyzing elements would be anisotropic themselves, see Fig. 3a and 3b.

Considering wavelets with anisotropic scaling will not remedy the situation, since within one fixed scale one cannot control the direction of the (now anisotrop-

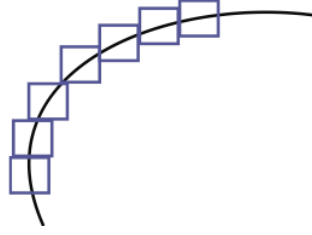


Fig. 3a Isotropic elements capturing a discontinuity curve.

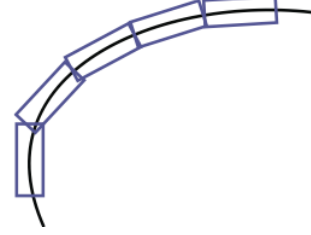


Fig. 3b Rotated, anisotropic elements capturing a discontinuity curve.

ically shaped) elements. Thus, to capture a discontinuity curve as in Fig. 3b, one needs not only anisotropic elements, but also a location parameter to locate the elements on the curve and a rotation parameter to align the elongated elements in the direction of the curve.

Let us finally remark why a parabolic scaling matrix $\text{diag}(2^j, 2^{j/2})$ will be natural to use as anisotropic scaling. Since the discontinuity curves of cartoon-like images are C^2 -smooth with bounded curvature, we may write the curve locally by a Taylor expansion. Let's assume it has the form $(s, E(s))$ with

$$E(s) = E(s') + E'(s')s + E''(t)s^2$$

near $s = s'$ for some $|t| \in [s', s]$. Clearly, the translation parameter will be used to position the anisotropic element near $(s', E(s'))$, and the orientation parameter to align with $(1, E'(s')s)$. If the length of the element is l , then, due to the term $E''(t)s^2$, the most beneficial height would be l^2 . And, in fact, parabolic scaling yields precisely this relation, i.e.,

$$\text{height} \approx \text{length}^2.$$

Hence, the main idea in the following will be to design a system which consists of anisotropically shaped elements together with a directional parameter to achieve the optimal approximation rate for cartoon-like images.

4 Pyramid-Adapted Shearlet Systems

After we have set our benchmark for directional representation systems in the sense of stating an optimality criteria for sparse approximations of the cartoon-like image class $\mathcal{C}_L^2(\mathbb{R}^d)$, we next introduce classes of shearlet systems we claim behave optimally. As already mentioned in the introduction of this chapter, optimally sparse approximations were proven for a class of band-limited as well as of compactly supported shearlet frames. For the definition of cone-adapted discrete shearlets and, in particular, classes of band-limited as well as of compactly supported shearlet frames

leading to optimally sparse approximations, we refer to Chapter [1]. In this section, we present the definition of discrete shearlets in 3D, from which the mentioned definitions in the 2D situation can also be directly concluded. As special cases, we then introduce particular classes of band-limited as well as of compactly supported shearlet frames, which will be shown to provide optimally approximations of $\mathcal{E}_L^2(\mathbb{R}^3)$ and, with a slight modification which we will elaborate on in Sect. 5.2.4, also for $\mathcal{E}_{\alpha,L}^\beta(\mathbb{R}^3)$ with $1 < \alpha \leq \beta \leq 2$.

4.1 General Definition

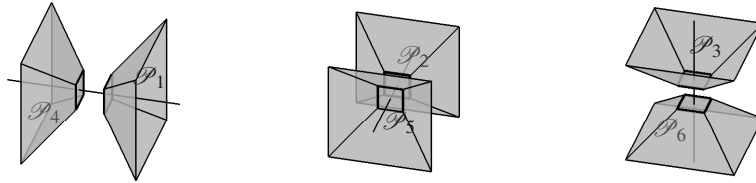
The first step in the definition of cone-adapted discrete 2D shearlets was a partitioning of 2D frequency domain into two pairs of high-frequency cones and one low-frequency rectangle. We mimic this step by partitioning 3D frequency domain into the three pairs of *pyramids* given by

$$\begin{aligned}\mathcal{P} &= \{(\xi_1, \xi_2, \xi_3) \in \mathbb{R}^3 : |\xi_1| \geq 1, |\xi_2/\xi_1| \leq 1, |\xi_3/\xi_1| \leq 1\}, \\ \tilde{\mathcal{P}} &= \{(\xi_1, \xi_2, \xi_3) \in \mathbb{R}^3 : |\xi_2| \geq 1, |\xi_1/\xi_2| \leq 1, |\xi_3/\xi_2| \leq 1\}, \\ \check{\mathcal{P}} &= \{(\xi_1, \xi_2, \xi_3) \in \mathbb{R}^3 : |\xi_3| \geq 1, |\xi_1/\xi_3| \leq 1, |\xi_2/\xi_3| \leq 1\},\end{aligned}$$

and the centered cube

$$\mathcal{C} = \{(\xi_1, \xi_2, \xi_3) \in \mathbb{R}^3 : \|(\xi_1, \xi_2, \xi_3)\|_\infty < 1\}.$$

This partition is illustrated in Fig. 4 which depicts the three pairs of pyramids and



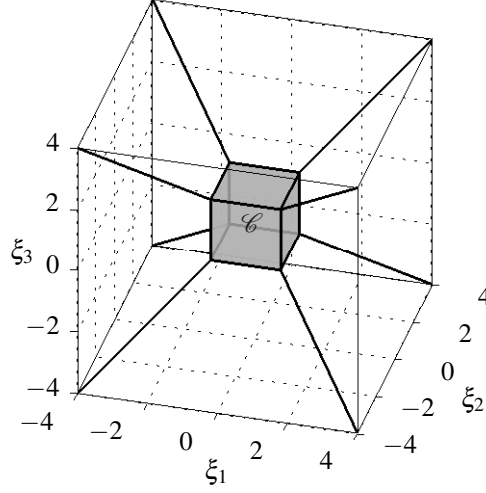
(a) Pyramid $\mathcal{P} = \mathcal{P}_1 \cup \mathcal{P}_4$ and the ξ_1 axis. (b) Pyramid $\tilde{\mathcal{P}} = \mathcal{P}_2 \cup \mathcal{P}_5$ and the ξ_2 axis. (c) Pyramids $\check{\mathcal{P}} = \mathcal{P}_3 \cup \mathcal{P}_6$ and the ξ_3 axis.

Fig. 4 The partition of the frequency domain: The ‘top’ of the six pyramids.

Fig. 5 depicting the centered cube surrounded by the three pairs of pyramids \mathcal{P} , $\tilde{\mathcal{P}}$, and $\check{\mathcal{P}}$.

The partitioning of frequency space into pyramids allows us to restrict the range of the shear parameters. Without such a partitioning as, e.g., in shearlet systems arising from the shearlet group, one must allow arbitrarily large shear parameters,

Fig. 5 The partition of the frequency domain: The centered cube \mathcal{C} . The arrangement of the six pyramids is indicated by the ‘diagonal’ lines. See Fig. 4 for a sketch of the pyramids.



which leads to a treatment biased towards one axis. The defined partition however enables restriction of the shear parameters to $[-\lceil 2^{j/2} \rceil, \lceil 2^{j/2} \rceil]$, similar to the definition of cone-adapted discrete shearlet systems. We would like to emphasize that this approach is key to provide an almost uniform treatment of different directions in a sense of a ‘good’ approximation to rotation.

Pyramid-adapted discrete shearlets are scaled according to the *paraboloidal scaling matrices* A_{2^j} , \tilde{A}_{2^j} or \check{A}_{2^j} , $j \in \mathbb{Z}$ defined by

$$A_{2^j} = \begin{pmatrix} 2^j & 0 & 0 \\ 0 & 2^{j/2} & 0 \\ 0 & 0 & 2^{j/2} \end{pmatrix}, \quad \tilde{A}_{2^j} = \begin{pmatrix} 2^{j/2} & 0 & 0 \\ 0 & 2^j & 0 \\ 0 & 0 & 2^{j/2} \end{pmatrix}, \quad \text{and} \quad \check{A}_{2^j} = \begin{pmatrix} 2^{j/2} & 0 & 0 \\ 0 & 2^{j/2} & 0 \\ 0 & 0 & 2^j \end{pmatrix},$$

and directionality is encoded by the *shear matrices* S_k , \tilde{S}_k , or \check{S}_k , $k = (k_1, k_2) \in \mathbb{Z}^2$, given by

$$S_k = \begin{pmatrix} 1 & k_1 & k_2 \\ 0 & 1 & 0 \\ 0 & 0 & 1 \end{pmatrix}, \quad \tilde{S}_k = \begin{pmatrix} 1 & 0 & 0 \\ k_1 & 1 & k_2 \\ 0 & 0 & 1 \end{pmatrix}, \quad \text{and} \quad \check{S}_k = \begin{pmatrix} 1 & 0 & 0 \\ 0 & 1 & 0 \\ k_1 & k_2 & 1 \end{pmatrix},$$

respectively. The reader should note that these definitions are (discrete) special cases of the general setup in [2]. The translation lattices will be defined through the following matrices: $M_c = \text{diag}(c_1, c_2, c_2)$, $\tilde{M}_c = \text{diag}(c_2, c_1, c_2)$, and $\check{M}_c = \text{diag}(c_2, c_2, c_1)$, where $c_1 > 0$ and $c_2 > 0$.

We are now ready to introduce 3D shearlet systems, for which we will make use of the vector notation $|k| \leq K$ for $k = (k_1, k_2)$ and $K > 0$ to denote $|k_1| \leq K$ and $|k_2| \leq K$.

Definition 2. For $c = (c_1, c_2) \in (\mathbb{R}_+)^2$, the *pyramid-adapted discrete shearlet system* $SH(\phi, \psi, \tilde{\psi}, \check{\psi}; c)$ generated by $\phi, \psi, \tilde{\psi}, \check{\psi} \in L^2(\mathbb{R}^3)$ is defined by

$$SH(\phi, \psi, \tilde{\psi}, \check{\psi}; c) = \Phi(\phi; c_1) \cup \Psi(\psi; c) \cup \tilde{\Psi}(\tilde{\psi}; c) \cup \check{\Psi}(\check{\psi}; c),$$

where

$$\begin{aligned} \Phi(\phi; c_1) &= \{\phi_m = \phi(\cdot - m) : m \in c_1 \mathbb{Z}^3\}, \\ \Psi(\psi; c) &= \{\psi_{j,k,m} = 2^j \psi(S_k A_{2^j} \cdot -m) : j \geq 0, |k| \leq \lceil 2^{j/2} \rceil, m \in M_c \mathbb{Z}^3\}, \\ \tilde{\Psi}(\tilde{\psi}; c) &= \{\tilde{\psi}_{j,k,m} = 2^j \tilde{\psi}(\tilde{S}_k \tilde{A}_{2^j} \cdot -m) : j \geq 0, |k| \leq \lceil 2^{j/2} \rceil, m \in \tilde{M}_c \mathbb{Z}^3\}, \end{aligned}$$

and

$$\check{\Psi}(\check{\psi}; c) = \{\check{\psi}_{j,k,m} = 2^j \check{\psi}(\check{S}_k \check{A}_{2^j} \cdot -m) : j \geq 0, |k| \leq \lceil 2^{j/2} \rceil, m \in \check{M}_c \mathbb{Z}^3\},$$

where $j \in \mathbb{N}_0$ and $k \in \mathbb{Z}^2$. For the sake of brevity, we will sometimes also use the notation ψ_λ with $\lambda = (j, k, m)$.

We now focus on two different special classes of pyramid-adapted discrete shearlets leading to the class of band-limited shearlets and the class of compactly supported shearlets for which optimality of their approximation properties with respect to cartoon-like images will be proven in Sect. 5.

4.2 Band-Limited 3D Shearlets

Let the shearlet generator $\psi \in L^2(\mathbb{R}^3)$ be defined by

$$\hat{\psi}(\xi) = \hat{\psi}_1(\xi_1) \hat{\psi}_2\left(\frac{\xi_2}{\xi_1}\right) \hat{\psi}_2\left(\frac{\xi_3}{\xi_1}\right), \quad (11)$$

where ψ_1 and ψ_2 satisfy the following assumptions:

- (i) $\hat{\psi}_1 \in C^\infty(\mathbb{R})$, $\text{supp } \hat{\psi}_1 \subset [-4, -\frac{1}{2}] \cup [\frac{1}{2}, 4]$, and

$$\sum_{j \geq 0} |\hat{\psi}_1(2^{-j} \xi)|^2 = 1 \quad \text{for } |\xi| \geq 1, \xi \in \mathbb{R}. \quad (12)$$

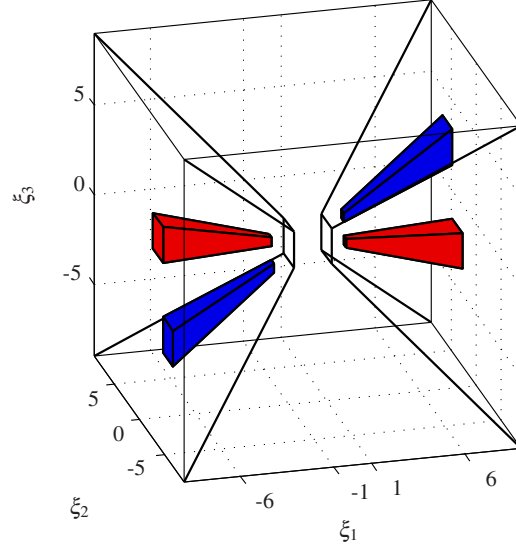
- (ii) $\hat{\psi}_2 \in C^\infty(\mathbb{R})$, $\text{supp } \hat{\psi}_2 \subset [-1, 1]$, and

$$\sum_{l=-1}^1 |\hat{\psi}_2(\xi + l)|^2 = 1 \quad \text{for } |\xi| \leq 1, \xi \in \mathbb{R}. \quad (13)$$

Thus, in frequency domain, the band-limited function $\psi \in L^2(\mathbb{R}^3)$ is almost a tensor product of one wavelet with two ‘bump’ functions, thereby a canonical generaliza-

tion of the classical band-limited 2D shearlets, see also Chapter [1]. This implies the support in frequency domain to have a needle-like shape with the wavelet acting in radial direction ensuring high directional selectivity, see also Fig. 6. The deriva-

Fig. 6 Support of two shearlet elements $\psi_{j,k,m}$ in the frequency domain. The two shearlet elements have the same scale parameter $j = 2$, but different shearing parameters $k = (k_1, k_2)$.



tion from being a tensor product, i.e., the substitution of ξ_2 and ξ_3 by the quotients ξ_2/ξ_1 and ξ_3/ξ_1 , respectively, in fact ensures a favorable behavior with respect to the shearing operator, and thus a tiling of frequency domain which leads to a tight frame for $L^2(\mathbb{R}^3)$.

A first step towards this result is the following observation.

Theorem 2 ([11]). *Let ψ be a band-limited shearlet defined as in this subsection. Then the family of functions*

$$\Psi(\psi) = \{\psi_{j,k,m} : j \geq 0, |k| \leq \lceil 2^{j/2} \rceil, m \in \frac{1}{8}\mathbb{Z}^3\}$$

forms a tight frame for $\check{L}^2(\mathcal{P}) := \{f \in L^2(\mathbb{R}^3) : \text{supp } \hat{f} \subset \mathcal{P}\}$.

Proof. For each $j \geq 0$, equation (13) implies that

$$\sum_{k=-\lceil 2^{j/2} \rceil}^{\lceil 2^{j/2} \rceil} |\hat{\psi}_2(2^{j/2}\xi + k)|^2 = 1, \quad \text{for } |\xi| \leq 1.$$

Hence, using equation (12), we obtain

$$\sum_{j \geq 0} \sum_{k_1, k_2 = -\lceil 2^{j/2} \rceil}^{\lceil 2^{j/2} \rceil} |\hat{\psi}(S_k^T A_{2^j}^{-1} \xi)|^2$$

$$\begin{aligned}
&= \sum_{j \geq 0} |\hat{\psi}_1(2^{-j}\xi_1)|^2 \sum_{k_1 = -\lceil 2^{j/2} \rceil}^{\lceil 2^{j/2} \rceil} |\hat{\psi}_2(2^{j/2} \frac{\xi_2}{\xi_1} + k_1)|^2 \sum_{k_2 = -\lceil 2^{j/2} \rceil}^{\lceil 2^{j/2} \rceil} |\hat{\psi}_2(2^{j/2} \frac{\xi_2}{\xi_1} + k_2)|^2 \\
&= 1,
\end{aligned}$$

for $\xi = (\xi_1, \xi_2, \xi_3) \in \mathcal{P}$. Using this equation together with the fact that $\hat{\psi}$ is supported inside $[-4, 4]^3$ proves the theorem. \square

By Thm. 2 and a change of variables, we can construct shearlet frames for $\check{L}^2(\mathcal{P})$, $\check{L}^2(\mathcal{S})$, and $\check{L}^2(\mathcal{J})$, respectively. Furthermore, wavelet theory provides us with many choices of $\phi \in L^2(\mathbb{R}^3)$ such that $\Phi(\phi; \frac{1}{8})$ forms a frame for $\check{L}^2(\mathcal{C})$. Since $\mathbb{R}^3 = \mathcal{C} \cup \mathcal{P} \cup \mathcal{S} \cup \mathcal{J}$ as a disjoint union, we can express any function $f \in L^2(\mathbb{R}^3)$ as $f = P_{\mathcal{C}}f + P_{\mathcal{P}}f + P_{\mathcal{S}}f + P_{\mathcal{J}}f$, where each component corresponds to the orthogonal projection of f onto one of the three pairs of pyramids or the centered cube in the frequency space. We then expand each of these components in terms of the corresponding tight frame. Finally, our representation of f will then be the sum of these four expansions. We remark that the projection of f onto the four subspaces can lead to artificially slow decaying shearlet coefficients; this will, e.g., be the case if f is in the Schwartz class. This problem does in fact not occur in the construction of compactly supported shearlets.

4.3 Compactly Supported 3D Shearlets

It is easy to see that the general form (11) does never lead to a function which is compactly supported in spatial domain. Thus, we need to deviate this form by now taking indeed exact tensor products as our shearlet generators, which has the additional benefit of leading to fast algorithmic realizations. This however causes the problem that the shearlets do not behave as favorable with respect to the shearing operator as in the previous subsection, and the question arises whether they actually do lead to at least a frame for $L^2(\mathbb{R}^3)$. The next results shows this to be true for an even much more general form of shearlet generators including compactly supported separable generators. The attentive reader will notice that this theorem even covers the class of band-limited shearlets introduced in Sect. 4.2.

Theorem 3 ([15]). *Let $\phi, \psi \in L^2(\mathbb{R}^3)$ be functions such that*

$$|\hat{\phi}(\xi)| \leq C_1 \min\{1, |\xi_1|^{-\gamma}\} \cdot \min\{1, |\xi_2|^{-\gamma}\} \cdot \min\{1, |\xi_3|^{-\gamma}\},$$

and

$$|\hat{\psi}(\xi)| \leq C_2 \cdot \min\{1, |\xi_1|^{\delta}\} \cdot \min\{1, |\xi_1|^{-\gamma}\} \cdot \min\{1, |\xi_2|^{-\gamma}\} \cdot \min\{1, |\xi_3|^{-\gamma}\},$$

for some constants $C_1, C_2 > 0$ and $\delta > 2\gamma > 6$. Define $\tilde{\psi}(x) = \psi(x_2, x_1, x_3)$ and $\check{\psi}(x) = \psi(x_3, x_2, x_1)$ for $x = (x_1, x_2, x_3) \in \mathbb{R}^3$. Then there exists a constant $c_0 > 0$

such that the shearlet system $SH(\phi, \psi, \tilde{\psi}, \check{\psi}; c)$ forms a frame for $L^2(\mathbb{R}^3)$ for all $c = (c_1, c_2)$ with $c_2 \leq c_1 \leq c_0$ provided that there exists a positive constant $M > 0$ such that

$$|\hat{\phi}(\xi)|^2 + \sum_{j \geq 0} \sum_{k_1, k_2 \in K_j} |\hat{\psi}(S_k^T A_{2^j} \xi)|^2 + |\hat{\tilde{\psi}}(\tilde{S}_k^T \tilde{A}_{2^j} \xi)|^2 + |\hat{\check{\psi}}(\check{S}_k^T \check{A}_{2^j} \xi)|^2 > M \quad (14)$$

for a.e $\xi \in \mathbb{R}^3$, where $K_j := [-\lceil 2^{j/2} \rceil, \lceil 2^{j/2} \rceil]$.

We next provide an example of a family of compactly supported shearlets satisfying the assumptions of Thm. 3. However, for applications, one is typically not only interested in whether a system forms a frame, but in the ratio of the associated frame bounds. In this regard, these shearlets also admit a theoretically derived estimate for this ratio which is reasonably close to 1, i.e., to being tight. The numerically derived ratio is even significantly closer as expected.

Example 1. Let $K, L \in \mathbb{N}$ be such that $L \geq 10$ and $\frac{3L}{2} \leq K \leq 3L - 2$, and define a shearlet $\psi \in L^2(\mathbb{R}^3)$ by

$$\hat{\psi}(\xi) = m_1(4\xi_1) \hat{\phi}(\xi_1) \hat{\phi}(2\xi_2) \hat{\phi}(2\xi_3), \quad \xi = (\xi_1, \xi_2, \xi_3) \in \mathbb{R}^3, \quad (15)$$

where the function m_0 is the low pass filter satisfying

$$|m_0(\xi_1)|^2 = \cos^{2K}(\pi\xi_1) \sum_{n=0}^{L-1} \binom{K-1+n}{n} \sin^{2n}(\pi\xi_1),$$

for $\xi_1 \in \mathbb{R}$, the function m_1 is the associated bandpass filter defined by

$$|m_1(\xi_1)|^2 = |m_0(\xi_1 + 1/2)|^2, \quad \xi_1 \in \mathbb{R},$$

and ϕ the scaling function is given by

$$\hat{\phi}(\xi_1) = \prod_{j=0}^{\infty} m_0(2^{-j}\xi_1), \quad \xi_1 \in \mathbb{R}.$$

In [13, 15] it is shown that ϕ and ψ indeed are compactly supported. Moreover, we have the following result.

Theorem 4 ([15]). Suppose $\psi \in L^2(\mathbb{R}^3)$ is defined as in (15). Then there exists a sampling constant $c_0 > 0$ such that the shearlet system $\Psi(\psi; c)$ forms a frame for $\check{L}^2(\mathcal{P})$ for any translation matrix M_c with $c = (c_1, c_2) \in (\mathbb{R}_+)^2$ and $c_2 \leq c_1 \leq c_0$.

Proof (sketch). Using upper and lower estimates of the absolute value of the trigonometric polynomial m_0 (cf. [5, 13]), one can show that ψ satisfies the hypothesis of Thm. 3 as well as

$$\sum_{j \geq 0} \sum_{k_1, k_2 \in K_j} |\hat{\psi}(S_k^T A_{2^j} \xi)|^2 > M \quad \text{for all } \xi \in \mathcal{P},$$

where $M > 0$ is a constant, for some sufficiently small $c_0 > 0$. We note that this inequality is an analog to (14) for the pyramid \mathcal{P} . Hence, by a result similar to Thm. 3, but for the case, where we restrict to the pyramid $\check{L}^2(\mathcal{P})$, it then follows that $\Psi(\psi; c)$ is a frame.

To obtain a frame for all of $L^2(\mathbb{R}^3)$ we simply set $\tilde{\psi}(x) = \psi(x_2, x_1, x_3)$ and $\check{\psi}(x) = \psi(x_3, x_2, x_1)$ as in Thm. 3, and choose $\phi(x) = \phi(x_1)\phi(x_2)\phi(x_3)$ as scaling function for $x = (x_1, x_2, x_3) \in \mathbb{R}^3$. Then the corresponding shearlet system $SH(\phi, \psi, \tilde{\psi}, \check{\psi}; c, \alpha)$ forms a frame for $L^2(\mathbb{R}^3)$. The proof basically follows from Daubechies' classical estimates for wavelet frames in [5, §3.3.2] and the fact that anisotropic and sheared windows obtained by applying the scaling matrix A_{2^j} and the shear matrix S_k^T to the effective support¹ of $\hat{\psi}$ cover the pyramid \mathcal{P} in the frequency domain. The same arguments can be applied to each of shearlet generators ψ , $\tilde{\psi}$ and $\check{\psi}$ as well as the scaling function ϕ to show a covering of the entire frequency domain and thereby the frame property of the pyramid-adapted shearlet system for $L^2(\mathbb{R}^3)$. We refer to [15] for the detailed proof.

Theoretical and numerical estimates of frame bounds for a particular parameter choice are shown in Table 1. We see that the theoretical estimates are overly pessimistic, since they are a factor 20 larger than the numerical estimated frame bound ratios. We mention that for 2D the estimated frame bound ratios are approximately 1/10 of the ratios found in Table 1.

Table 1 Frame bound ratio for the shearlet frame from Example 1 with parameters $K = 39, L = 19$.

| Theoretical (B/A) | Numerical (B/A) | Translation constants (c_1, c_2) |
|-----------------------|---------------------|--------------------------------------|
| 345.7 | 13.42 | (0.9, 0.25) |
| 226.6 | 13.17 | (0.9, 0.20) |
| 226.4 | 13.16 | (0.9, 0.15) |
| 226.4 | 13.16 | (0.9, 0.10) |

4.4 Some Remarks on Construction Issues

The compactly supported shearlets $\psi_{j,k,m}$ from Example 1 are, in spatial domain, of size $2^{-j/2}$ times $2^{-j/2}$ times 2^{-j} due to the scaling matrix A_{2^j} . This reveals that the shearlet elements will become ‘plate-like’ as $j \rightarrow \infty$. For an illustration, we refer to Fig. 7. Band-limited shearlets, on the other hand, do not have compactly support, but their effective support (the region where the energy of the function is concentrated) in spatial domain will likewise be of size $2^{-j/2}$ times $2^{-j/2}$ times 2^{-j} owing to their smoothness in frequency domain. Contemplating about the fact that intuitively

¹ Loosely speaking, we say that $f \in L^2(\mathbb{R}^d)$ has *effective* support on B if the ratio $\|f\chi_B\|_{L^2} / \|f\|_{L^2}$ is ‘close’ to 1.

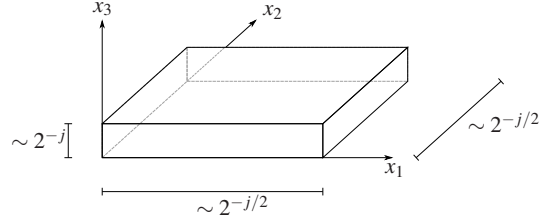


Fig. 7 Support of a shearlet $\tilde{\psi}_{j,0,m}$ from Example 1.

such shearlet elements should provide sparse approximations of surface singularities, one could also think of using the scaling matrix $A_{2^j} = \text{diag}(2^j, 2^j, 2^{j/2})$ with similar changes for \tilde{A}_{2^j} and \check{A}_{2^j} to derive ‘needle-like’ shearlet elements in space domain. These would intuitively behave favorable with respect to the other type of anisotropic features occurring in 3D, that is curvilinear singularities. Surprisingly, we will show in Sect. 5.2 that for optimally sparse approximation plate-like shearlets, i.e., shearlets associated with scaling matrix $A_{2^j} = \text{diag}(2^j, 2^{j/2}, 2^{j/2})$, and similarly \tilde{A}_{2^j} and \check{A}_{2^j} are sufficient.

Let us also mention that, more generally, non-paraboloidal scaling matrices of the form $A_j = \text{diag}(2^j, 2^{a_1 j}, 2^{a_2 j})$ for $0 < a_1, a_2 \leq 1$ can be considered. The parameters a_1 and a_2 allow precise control of the aspect ratio of the shearlet elements, ranging from very plate-like to very needle-like, according to the application at hand, i.e., choosing the shearlet-shape that is the best matches the geometric characteristics of the considered data. The case $a_i < 1$ is covered by the setup of the multidimensional shearlet transform explained in Chapter [2].

Let us finish this section with a general thought on the construction of band-limited (not separable) tight shearlet frames versus compactly supported (non-tight, but separable) shearlet frames. It seems that there is a trade-off between *compact support* of the shearlet generators, *tightness* of the associated frame, and *separability* of the shearlet generators. In fact, even in 2D, all known constructions of tight shearlet frames do not use separable generators, and these constructions can be shown to *not* be applicable to compactly supported generators. Presumably, tightness is difficult to obtain while allowing for compactly supported generators, but we can gain separability which leads to fast algorithmic realizations, see Chapter [3]. If we though allow non-compactly supported generators, tightness is possible as shown in Sect. 4.2, but separability seems to be out of reach, which causes problems for fast algorithmic realizations.

5 Optimal Sparse Approximations

In this section, we will show that shearlets – both band-limited as well as compactly supported as defined in Sect. 4 – indeed provide the optimal sparse approximation rate for cartoon-like images from Sect. 3.2. Thus, letting $(\psi_\lambda)_\lambda = (\psi_{j,k,m})_{j,k,m}$ denote the band-limited shearlet frame from Sect. 4.2 and the compactly supported

shearlet frame from Sect. 4.3 in both 2D and 3D (see [1]) and $d \in \{2, 3\}$, we aim to prove that

$$\|f - f_N\|_{L^2}^2 \lesssim N^{-\frac{2}{d-1}} \quad \text{for all } f \in \mathcal{E}_L^2(\mathbb{R}^d),$$

where – as debated in Sect. 3.1 – f_N denotes the N -term approximation using the N largest coefficients as in (5). Hence, in 2D we aim for the rate N^{-2} and in 3D we aim for the rate N^{-1} with ignoring log-factors. As mentioned in Sect. 3.2, see (10), in order to prove these rate, it suffices to show that the n th largest shearlet coefficient c_n^* decays as

$$|c_n^*| \lesssim n^{-\frac{d+1}{2(d-1)}} = \begin{cases} n^{-3/2} & : d = 2, \\ n^{-1} & : d = 3. \end{cases}$$

According to Dfn. 1 this will show that among all adaptive and non-adaptive representation systems shearlet frames behave optimal with respect to sparse approximation of cartoon-like images. That one is able to obtain such an optimal approximation error rate might seem surprising, since the shearlet system as well as the approximation procedure will be non-adaptive.

To present the necessary hypotheses, illustrate the key ideas of the proofs, and debate the differences between the arguments for band-limited and compactly supported shearlets, we first focus on the situation of 2D shearlets. We then discuss the 3D situation, with a sparsified proof, mainly discussing the essential differences to the proof for 2D shearlets and highlighting the crucial nature of this case (cf. Sect. 1.3).

5.1 Optimal Sparse Approximations in 2D

As discussed in the previous section, in the case $d = 2$, we aim for the estimates $|c_n^*| \lesssim n^{-3/2}$ and $\|f - f_N\|_{L^2}^2 \lesssim N^{-2}$ (up to log-factors). In Sect. 5.1.1 we will first provide a heuristic analysis to argue that shearlet frames indeed can deliver these rates. In Sect. 5.1.2 and 5.1.3 we then discuss the required hypotheses and state the main optimality result. The subsequent subsections are then devoted to proving the main result.

5.1.1 A Heuristic Analysis

We start by giving a heuristic argument (inspired by a similar argument for curvelets in [4]) on why the error $\|f - f_N\|_{L^2}^2$ satisfies the asymptotic rate N^{-2} . We emphasize that this heuristic argument applies to both the band-limited and also the compactly supported case.

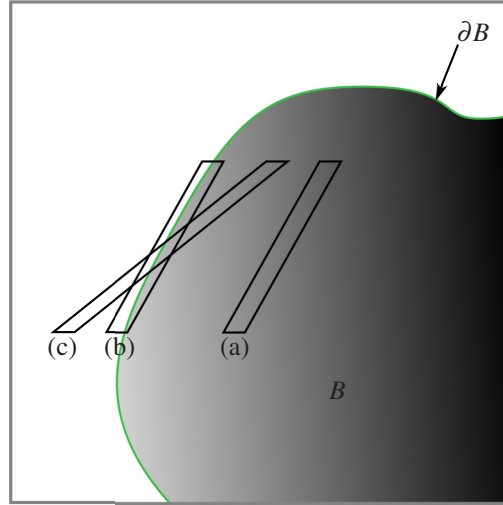
For simplicity we assume $L = 1$, and let $f \in \mathcal{E}_L^2(\mathbb{R}^2)$ be a 2D cartoon-like image. The main concern is to derive the estimate (19) for the shearlet coefficients $\langle f, \hat{\psi}_{j,k,m} \rangle$, where $\hat{\psi}$ denotes either ψ or $\tilde{\psi}$. We consider only the case $\hat{\psi} = \psi$, since

the other case can be handled similarly. For compactly supported shearlet, we can think of our generators having the form $\psi(x) = \eta(x_1)\phi(x_2)$, $x = (x_1, x_2)$, where η is a wavelet and ϕ a bump (or a scaling) function. It will become important, that the wavelet ‘points’ in the x_1 -axis direction, which corresponds to the ‘short’ direction of the shearlet. For band-limited generators, we can think of our generators having the form $\hat{\psi}(\xi) = \hat{\eta}(\xi_2/\xi_1)\hat{\phi}(\xi_2)$ for $\xi = (\xi_1, \xi_2)$. We, moreover, restrict our analysis to shearlets $\psi_{j,k,m}$ since the frame elements $\tilde{\psi}_{j,k,m}$ can be handled in a similar way.

We now consider three cases of coefficients $\langle f, \psi_{j,k,m} \rangle$:

- (a) Shearlets $\psi_{j,k,m}$ whose support does not overlap with the boundary ∂B .
- (b) Shearlets $\psi_{j,k,m}$ whose support overlaps with ∂B and is nearly tangent.
- (c) Shearlets $\psi_{j,k,m}$ whose support overlaps with ∂B , but not tangentially.

Fig. 8 Sketch of the three cases: (a) the support of $\psi_{j,k,m}$ does not overlap with ∂B , (b) the support of $\psi_{j,k,m}$ does overlap with ∂B and is nearly tangent, (c) the support of $\psi_{j,k,m}$ does overlap with ∂B , but not tangentially. Note that only a section of the discontinuity curve ∂B is shown, and that for the case of band-limited shearlets only the effective support is shown.



It turns out that only coefficients from case (b) will be significant. Case (b) is, loosely speaking, the situation, where the wavelet η crosses the discontinuity curve over the entire ‘height’ of the shearlet, see Fig. 8.

Case (a). Since f is C^2 -smooth away from ∂B , the coefficients $|\langle f, \psi_{j,k,m} \rangle|$ will be sufficiently small owing to the approximation property of the wavelet η . The situation is sketched in Fig. 8.

Case (b). At scale $j > 0$, there are about $O(2^{j/2})$ coefficients, since the shearlet elements are of length $2^{-j/2}$ (and ‘thickness’ 2^{-j}) and the length of ∂B is finite. By Hölder’s inequality, we immediately obtain

$$|\langle f, \psi_{j,k,m} \rangle| \leq \|f\|_{L^\infty} \|\psi_{j,k,m}\|_{L^1} \leq C_1 2^{-3j/4} \|\psi\|_{L^1} \leq C_2 \cdot 2^{-3j/4}$$

for some constants $C_1, C_2 > 0$. In other words, we have $O(2^{j/2})$ coefficients bounded by $C_2 \cdot 2^{-3j/4}$. Assuming the case (a) and (c) coefficients are negligible, the n th

largest coefficient c_n^* is then bounded by

$$|c_n^*| \leq C \cdot n^{-3/2},$$

which was what we aimed to show; compare to (8) in Dfn. 1. This in turn implies (cf. estimate (9)) that

$$\sum_{n>N} |c_n^*|^2 \leq \sum_{n>N} C \cdot n^{-3} \leq C \cdot \int_N^\infty x^{-3} dx \leq C \cdot N^{-2}.$$

By Lemma 1, as desired it follows that

$$\|f - f_N\|_{L^2}^2 \leq \frac{1}{A} \sum_{n>N} |c_n^*|^2 \leq C \cdot N^{-2},$$

where A denotes the lower frame bound of the shearlet frame.

Case (c). Finally, when the shearlets are sheared away from the tangent position in case (b), they will again be small. This is due to the frequency support of f and ψ_λ as well as to the directional vanishing moment conditions assumed in Setup 1 or 2, which will be formally introduced in the next subsection.

Summarising our findings, we have argued, at least heuristically, that shearlet frames provide optimal sparse approximation of cartoon-like images as defined in Dfn. 1.

5.1.2 Required Hypotheses

After having build up some intuition on why the optimal sparse approximation rate is achievable using shearlets, we will now go into more details and discuss the hypotheses required for the main result. This will along the way already highlight some differences between the band-limited and compactly supported case.

For this discussion, assume that $f \in L^2(\mathbb{R}^2)$ is piecewise C^{L+1} -smooth with a discontinuity on the line $\mathcal{L} : x_1 = sx_2$, $s \in \mathbb{R}$, so that the function f is well approximated by two 2D polynomials of degree $L > 0$, one polynomial on either side of \mathcal{L} , and denote this piecewise polynomial $q(x_1, x_2)$. We denote the restriction of q to lines $x_1 = sx_2 + t$, $t \in \mathbb{R}$, by $p_t(x_2) = q(sx_2 + t, x_2)$. Hence, p_t is a 1D polynomial along lines parallel to \mathcal{L} going through $(x_1, x_2) = (t, 0)$; these lines are marked by dashed lines in Fig. 9b.

We now aim at estimating the absolute value of a shearlet coefficient $\langle f, \psi_{j,k,m} \rangle$ by

$$|\langle f, \psi_{j,k,m} \rangle| \leq |\langle q, \psi_{j,k,m} \rangle| + |\langle (q - f), \psi_{j,k,m} \rangle|. \quad (16)$$

We first observe that $|\langle f, \psi_{j,k,m} \rangle|$ will be small depending on the approximation quality of the (piecewise) polynomial q and the decay of ψ in the spatial domain. Hence it suffices to focus on estimating $|\langle q, \psi_{j,k,m} \rangle|$.

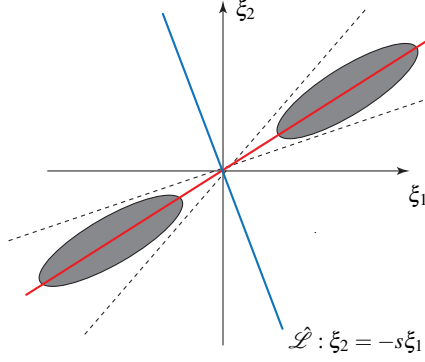


Fig. 9a Shaded region: The effective part of $\text{supp } \hat{\psi}_{j,k,m}$ in the frequency domain.

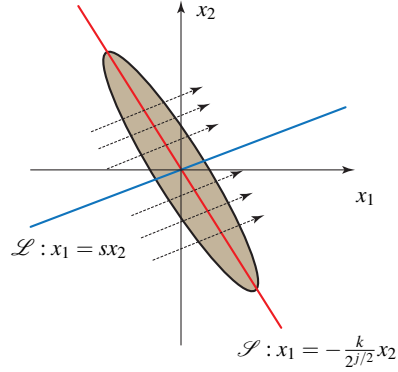


Fig. 9b Shaded region: The effective part of $\text{supp } \psi_{j,k,m}$ in the spatial domain. Dashed lines: the direction of line integration $I(t)$.

For this, let us consider the line integration along the direction $(x_1, x_2) = (s, 1)$ as follows: For $t \in \mathbb{R}$ fixed, define integration of $q\psi_{j,k,m}$ along the lines $x_1 = sx_2 + t$, $x_2 \in \mathbb{R}$, as

$$I(t) = \int_{\mathbb{R}} p_t(x_2) \psi_{j,k,m}(sx_2 + t, x_2) dx_2,$$

Observe that $|\langle q, \psi_{j,k,m} \rangle| = 0$ is equivalent to $I \equiv 0$. For simplicity, let us now assume $m = (0, 0)$. Then

$$\begin{aligned} I(t) &= 2^{\frac{3}{4}j} \int_{\mathbb{R}} p_t(x_2) \psi(S_k A_{2^j}(sx_2 + t, x_2)) dx_2 \\ &= 2^{\frac{3}{4}j} \sum_{\ell=0}^L c_\ell \int_{\mathbb{R}} x_2^\ell \psi(S_k A_{2^j}(sx_2 + t, x_2)) dx_2 \\ &= 2^{\frac{3}{4}j} \sum_{\ell=0}^L c_\ell \int_{\mathbb{R}} x_2^\ell \psi(A_{2^j} S_{k/2^{j/2}+s}(t, x_2)) dx_2, \end{aligned}$$

and, by the Fourier slice theorem [12] (see also (28)), it follows that

$$|I(t)| = 2^{\frac{3}{4}j} \left| \sum_{\ell=0}^L \frac{2^{-\frac{\ell}{2}j}}{(2\pi)^\ell} c_\ell \int_{\mathbb{R}} \left(\frac{\partial}{\partial \xi_2} \right)^\ell \hat{\psi}(A_{2^j}^{-1} S_{k/2^{j/2}+s}^{-T}(\xi_1, 0)) e^{2\pi i \xi_1 t} d\xi_1 \right|.$$

Note that

$$\int_{\mathbb{R}} \left(\frac{\partial}{\partial \xi_2} \right)^\ell \hat{\psi}(A_{2^j}^{-1} S_{k/2^{j/2}+s}^{-T}(\xi_1, 0)) e^{2\pi i \xi_1 t} d\xi_1 = 0 \quad \text{for almost all } t \in \mathbb{R}$$

if and only if

$$\left(\frac{\partial}{\partial \xi_2}\right)^\ell \hat{\psi}(A_{2^j}^{-1} S_{k/2^{j/2}+s}^{-T}(\xi_1, 0)) = 0 \quad \text{for almost all } \xi_1 \in \mathbb{R}.$$

Therefore, to ensure $I(t) = 0$ for any 1D polynomial p_t of degree $L > 0$, we require the following condition:

$$\left(\frac{\partial}{\partial \xi_2}\right)^\ell \hat{\psi}_{j,k,0}(\xi_1, -s\xi_1) = 0 \quad \text{for almost all } \xi_1 \in \mathbb{R} \text{ and } \ell = 0, \dots, L.$$

These are the so-called *directional vanishing moments* (cf. [7]) in the direction $(s, 1)$. We now consider the two cases, band-limited shearlets and compactly supported shearlets, separately.

If ψ is a band-limited shearlet generator, we automatically have

$$\left(\frac{\partial}{\partial \xi_2}\right)^\ell \hat{\psi}_{j,k,m}(\xi_1, -s\xi_1) = 0 \quad \text{for } \ell = 0, \dots, L \quad \text{if } |s + \frac{k}{2^{j/2}}| \geq 2^{-j/2}, \quad (17)$$

since $\text{supp } \hat{\psi} \subset \mathcal{D}$, where $\mathcal{D} = \{\xi \in \mathbb{R}^2 : |\xi_2/\xi_1| \leq 1\}$ as discussed in Chapter [1]. Observe that the ‘direction’ of $\text{supp } \psi_{j,k,m}$ is determined by the line $\mathcal{S} : x_1 = -\frac{k}{2^{j/2}}x_2$. Hence, equation (17) implies that, if the direction of $\text{supp } \psi_{j,k,m}$, i.e., of \mathcal{S} is *not* close to the direction of \mathcal{L} in the sense that $|s + \frac{k}{2^{j/2}}| \geq 2^{-j/2}$, then

$$|\langle q, \psi_{j,k,m} \rangle| = 0.$$

However, if ψ is a compactly supported shearlet generator, equation (17) can never hold, since it requires that $\text{supp } \hat{\psi} \subset \mathcal{D}$. Therefore, for compactly supported generators, we will assume that $(\frac{\partial}{\partial \xi_2})^l \hat{\psi}$, $l = 0, 1$, has sufficient decay in \mathcal{D}^c to force $I(t)$ and hence $|\langle q, \psi_{j,k,m} \rangle|$ to be sufficiently small. It should be emphasized that the drawback that $I(t)$ will only be ‘small’ for compactly supported shearlets (due to the lack of exact directional vanishing moments) will be compensated by the perfect localization property which still enables optimal sparsity.

Thus, the developed conditions ensure that both terms on the right hand side of (16) can be effectively bounded.

This discussion gives naturally rise to the following hypotheses for optimal sparse approximation. Let us start with the hypotheses for the band-limited case.

Setup 1. The generators $\phi, \psi, \tilde{\psi} \in L^2(\mathbb{R}^2)$ are band-limited and C^∞ in the frequency domain. Furthermore, the shearlet system $SH(\phi, \psi, \tilde{\psi}; c)$ forms a frame for $L^2(\mathbb{R}^2)$ (cf. the construction in Chapter [1] or Sect. 4.2).

In contrast to this, the conditions for the compactly supported shearlets are as follows:

Setup 2. The generators $\phi, \psi, \tilde{\psi} \in L^2(\mathbb{R}^2)$ are compactly supported, and the shearlet system $SH(\phi, \psi, \tilde{\psi}; c)$ forms a frame for $L^2(\mathbb{R}^2)$. Furthermore, for all $\xi = (\xi_1, \xi_2) \in \mathbb{R}^2$, the function ψ satisfies

- (i) $|\hat{\psi}(\xi)| \leq C \cdot \min\{1, |\xi_1|^\delta\} \cdot \min\{1, |\xi_1|^{-\gamma}\} \cdot \min\{1, |\xi_2|^{-\gamma}\}$, and
- (ii) $\left| \frac{\partial}{\partial \xi_2} \hat{\psi}(\xi) \right| \leq |h(\xi_1)| \left(1 + \frac{|\xi_2|}{|\xi_1|} \right)^{-\gamma},$

where $\delta > 6$, $\gamma \geq 3$, $h \in L^1(\mathbb{R})$, and C a constant, and $\tilde{\psi}$ satisfies analogous conditions with the obvious change of coordinates (cf. the construction in Sect. 4.3).

Conditions (i) and (ii) in Setup 2 are exactly the decay assumptions on $(\frac{\partial}{\partial \xi_2})^l \hat{\psi}$, $l = 0, 1$, discussed above that guarantees control of the size of $I(t)$.

5.1.3 Main Result

We are now ready to present the main result, which states that under Setup 1 or Setup 2 shearlets provide optimally sparse approximations for cartoon-like images.

Theorem 5 ([10, 17]). *Assume Setup 1 or 2. Let $L \in \mathbb{N}$. For any $\nu > 0$ and $\mu > 0$, the shearlet frame $SH(\phi, \psi, \tilde{\psi}; c)$ provides optimally sparse approximations of functions $f \in \mathcal{E}_L^2(\mathbb{R}^2)$ in the sense of Dfn. 1, i.e.,*

$$\|f - f_N\|_{L^2}^2 = O(N^{-2}(\log N)^3), \quad \text{as } N \rightarrow \infty, \quad (18)$$

and

$$|c_n^*| \lesssim n^{-3/2}(\log n)^{3/2}, \quad \text{as } n \rightarrow \infty, \quad (19)$$

where $c = \{\langle f, \hat{\psi}_\lambda \rangle : \lambda \in \Lambda, \hat{\psi} = \psi \text{ or } \hat{\psi} = \tilde{\psi}\}$ and $c^* = (c_n^*)_{n \in \mathbb{N}}$ is a decreasing (in modulus) rearrangement of c .

5.1.4 Band-Limitedness versus Compactly Supportedness

Before we delve into the proof of Thm. 5, we first carefully discuss the main differences between band-limited shearlets and compactly supported shearlets which requires adaptations of the proof.

In the case of compactly supported shearlets, we can consider the two cases $|\text{supp } \hat{\psi}_\lambda \cap \partial B| \neq 0$ and $|\text{supp } \hat{\psi}_\lambda \cap \partial B| = 0$. In case the support of the shearlet intersects the discontinuity curve ∂B of the cartoon-like image f , we will estimate each shearlet coefficient $\langle f, \hat{\psi}_\lambda \rangle$ individually using the decay assumptions on $\hat{\psi}$ in Setup 2, and then apply a simple counting estimate to obtain the sought estimates (18) and (19). In the other case, in which the shearlet does not interact with

the discontinuity, we are simply estimating the decay of shearlet coefficients of a C^2 function. The argument here is similar to the approximation of smooth functions using wavelet frames and rely on estimating coefficients at all scales using the frame property.

In the case of band-limited shearlets, it is not allowed to consider two cases $|\text{supp } \psi_\lambda \cap \partial B| = 0$ and $|\text{supp } \psi_\lambda \cap \partial B| \neq 0$ separately, since all shearlet elements ψ_λ intersect the boundary of the set B . In fact, one needs to first localize the cartoon-like image f by compactly supported smooth window functions associated with dyadic squares using a partition of unity. Letting f_Q denote such a localized version, we then estimate $\langle f_Q, \psi_\lambda \rangle$ instead of directly estimating the shearlet coefficients $\langle f, \psi_\lambda \rangle$. Moreover, in the case of band-limited shearlets, one needs to estimate the sparsity of the sequence of the shearlet coefficients rather than analyzing the decay of individual coefficients.

In the next subsections we present the proof – first for band-limited, then for compactly supported shearlets – in the case $L = 1$, i.e., when the discontinuity curve in the model of cartoon-like images is smooth. Finally, the extension to $L \neq 1$ will be discussed for both cases simultaneously.

We will first, however, introduce some notation used in the proofs and prove a helpful lemma which will be used in both cases: band-limited and compactly supported shearlets. For a fixed j , we let \mathcal{Q}_j be a collection of dyadic squares defined by

$$\mathcal{Q}_j = \{Q = [\frac{l_1}{2^{j/2}}, \frac{l_1+1}{2^{j/2}}] \times [\frac{l_2}{2^{j/2}}, \frac{l_2+1}{2^{j/2}}] : l_1, l_2 \in \mathbb{Z}\}.$$

We let Λ denote the set of all indices (j, k, m) in the shearlet system and define

$$\Lambda_j = \{(j, k, m) \in \Lambda : -\lceil 2^{j/2} \rceil \leq k \leq \lceil 2^{j/2} \rceil, m \in \mathbb{Z}^2\}.$$

For $\varepsilon > 0$, we define the set of ‘relevant’ indices on scale j as

$$\Lambda_j(\varepsilon) = \{\lambda \in \Lambda_j : |\langle f, \psi_\lambda \rangle| > \varepsilon\}$$

and, on all scales, as

$$\Lambda(\varepsilon) = \{\lambda \in \Lambda : |\langle f, \psi_\lambda \rangle| > \varepsilon\}.$$

Lemma 2. *Assume Setup 1 or 2. Let $f \in \mathcal{E}_L^2(\mathbb{R}^2)$. Then the following assertions hold:*

(i) *For some constant C , we have*

$$\#\Lambda_j(\varepsilon) = 0 \quad \text{for } j \geq \frac{4}{3} \log_2(\varepsilon^{-1}) + C \quad (20)$$

(ii) *If*

$$\#\Lambda_j(\varepsilon) \lesssim \varepsilon^{-2/3}, \quad (21)$$

for $j \geq 0$, then

$$\#\Lambda(\varepsilon) \lesssim \varepsilon^{-2/3} \log_2(\varepsilon^{-1}), \quad (22)$$

which, in turn, implies (18) and (19).

Proof. (i). Since $\psi \in L^1(\mathbb{R}^2)$ for both the band-limited and compactly supported setup, we have that

$$\begin{aligned} |\langle f, \psi_\lambda \rangle| &= \left| \int_{\mathbb{R}^2} f(x) 2^{\frac{3j}{4}} \psi(S_k A_{2^j} x - m) dx \right| \\ &\leq 2^{\frac{3j}{4}} \|f\|_\infty \int_{\mathbb{R}^2} |\psi(S_k A_{2^j} x - m)| dx \\ &= 2^{-\frac{3j}{4}} \|f\|_\infty \|\psi\|_1. \end{aligned} \quad (23)$$

As a consequence, there is a scale j_ε such that $|\langle f, \psi_\lambda \rangle| < \varepsilon$ for each $j \geq j_\varepsilon$. It therefore follows from (23) that

$$\#\Lambda(\varepsilon) = 0 \quad \text{for } j > \frac{4}{3} \log_2(\varepsilon^{-1}) + C.$$

(ii). By assertion (i) and estimate (21), we have that

$$\#\Lambda(\varepsilon) \leq C \varepsilon^{-2/3} \log_2(\varepsilon^{-1}).$$

From this, the value ε can be written as a function of the total number of coefficients $n = \#\Lambda(\varepsilon)$. We obtain

$$\varepsilon(n) \leq C n^{-3/2} (\log_2(n))^{3/2} \quad \text{for sufficiently large } n.$$

This implies that

$$|c_n^*| \leq C n^{-3/2} (\log_2(n))^{3/2}$$

and

$$\sum_{n>N} |c_n^*|^2 \leq C N^{-2} (\log_2(N))^3 \quad \text{for sufficiently large } N > 0,$$

where c_n^* as usual denotes the n th largest shearlet coefficient in modulus. \square

5.1.5 Proof for Band-Limited Shearlets for $L = 1$

Since we assume $L = 1$, we have that $f \in \mathcal{E}_L^2(\mathbb{R}^2) = \mathcal{E}^2(\mathbb{R}^2)$. As mentioned in the previous section, we will now measure the sparsity of the shearlet coefficients $\{\langle f, \psi_\lambda \rangle : \lambda \in \Lambda\}$. For this, we will use the weak ℓ^p quasi norm $\|\cdot\|_{w\ell^p}$ defined as follows. For a sequence $s = (s_i)_{i \in I}$, we let, as usual, s_n^* be the n th largest coefficient in s in modulus. We then define:

$$\|s\|_{w\ell^p} = \sup_{n>0} n^{\frac{1}{p}} |s_n^*|.$$

One can show [19] that this definition is equivalent to

$$\|s\|_{w\ell^p} = \left(\sup \{ \# \{i : |s_i| > \varepsilon\} | \varepsilon^p : \varepsilon > 0 \} \right)^{\frac{1}{p}}.$$

We will only consider the case $\hat{\psi} = \psi$ since the case $\hat{\psi} = \tilde{\psi}$ can be handled similarly. To analyze the decay properties of the shearlet coefficients $(\langle f, \psi_\lambda \rangle)_\lambda$ at a given scale parameter $j \geq 0$, we smoothly localize the function f near dyadic squares. Fix the scale parameter $j \geq 0$. For a non-negative C^∞ function w with support in $[0, 1]^2$, we then define a smooth partition of unity

$$\sum_{Q \in \mathcal{Q}_j} w_Q(x) = 1, \quad x \in \mathbb{R}^2,$$

where, for each dyadic square $Q \in \mathcal{Q}_j$, $w_Q(x) = w(2^{j/2}x_1 - l_1, 2^{j/2}x_2 - l_2)$. We will then examine the shearlet coefficients of the localized function $f_Q := fw_Q$. With this smooth localization of the function f , we can now consider the two separate cases, $|\text{supp } w_Q \cap \partial B| = 0$ and $|\text{supp } w_Q \cap \partial B| \neq 0$. Let

$$\mathcal{Q}_j = \mathcal{Q}_j^0 \cup \mathcal{Q}_j^1,$$

where the union is disjoint and \mathcal{Q}_j^0 is the collection of those dyadic squares $Q \in \mathcal{Q}_j$ such that the edge curve ∂B intersects the support of w_Q . Since each Q has side length $2^{-j/2}$ and the edge curve ∂B has finite length, it follows that

$$\#|\mathcal{Q}_j^0| \lesssim 2^{j/2}. \quad (24)$$

Similarly, since f is compactly supported in $[0, 1]^2$, we see that

$$\#|\mathcal{Q}_j^1| \lesssim 2^j. \quad (25)$$

The following theorems analyze the sparsity of the shearlets coefficients for each dyadic square $Q \in \mathcal{Q}_j$.

Theorem 6 ([10]). *Let $f \in \mathcal{E}^2(\mathbb{R}^2)$. For $Q \in \mathcal{Q}_j^0$, with $j \geq 0$ fixed, the sequence of shearlet coefficients $\{d_\lambda := \langle f_Q, \psi_\lambda \rangle : \lambda \in \Lambda_j\}$ obeys*

$$\left\| (d_\lambda)_{\lambda \in \Lambda_j} \right\|_{w\ell^{2/3}} \lesssim 2^{-\frac{3j}{4}}.$$

Theorem 7 ([10]). *Let $f \in \mathcal{E}^2(\mathbb{R}^2)$. For $Q \in \mathcal{Q}_j^1$, with $j \geq 0$ fixed, the sequence of shearlet coefficients $\{d_\lambda := \langle f_Q, \psi_\lambda \rangle : \lambda \in \Lambda_j\}$ obeys*

$$\left\| (d_\lambda)_{\lambda \in \Lambda_j} \right\|_{w\ell^{2/3}} \lesssim 2^{-\frac{3j}{2}}.$$

As a consequence of these two theorems, we have the following result.

Theorem 8 ([10]). *Suppose $f \in \mathcal{E}^2(\mathbb{R}^2)$. Then, for $j \geq 0$, the sequence of the shearlet coefficients $\{c_\lambda := \langle f, \psi_\lambda \rangle : \lambda \in \Lambda_j\}$ obeys*

$$\left\| (c_\lambda)_{\lambda \in \Lambda_j} \right\|_{w\ell^{2/3}} \lesssim 1.$$

Proof. Using Thm. 6 and 7, by the p -triangle inequality for weak ℓ^p spaces, $p \leq 1$, we have

$$\begin{aligned} \|\langle f, \psi_\lambda \rangle\|_{w\ell^{2/3}}^{2/3} &\leq \sum_{Q \in \mathcal{Q}_j} \|\langle f_Q, \psi_\lambda \rangle\|_{w\ell^{2/3}}^{2/3} \\ &= \sum_{Q \in \mathcal{Q}_j^0} \|\langle f_Q, \psi_\lambda \rangle\|_{w\ell^{2/3}}^{2/3} + \sum_{Q \in \mathcal{Q}_j^1} \|\langle f_Q, \psi_\lambda \rangle\|_{w\ell^{2/3}}^{2/3} \\ &\leq C \#|\mathcal{Q}_j^0| 2^{-j/2} + C \#|\mathcal{Q}_j^1| 2^{-j}. \end{aligned}$$

Equations (24) and (25) complete the proof. \square

We can now prove Thm. 5 for the band-limited setup.

Proof (Thm. 5 for Setup 1). From Thm. 8, we have that

$$\#|\Lambda_j(\varepsilon)| \leq C\varepsilon^{-2/3},$$

for some constant $C > 0$, which, by Lemma 2, completes the proof. \square

5.1.6 Proof for Compactly Supported Shearlets for $L = 1$

To derive the sought estimates (18) and (19) for dimension $d = 2$, we will study two separate cases: Those shearlet elements ψ_λ which do not interact with the discontinuity curve, and those elements which do.

Case 1. The compact support of the shearlet ψ_λ does not intersect the boundary of the set B , i.e., $|\text{supp } \psi_\lambda \cap \partial B| = 0$.

Case 2. The compact support of the shearlet ψ_λ does intersect the boundary of the set B , i.e., $|\text{supp } \psi_\lambda \cap \partial B| \neq 0$.

For *Case 1* we will not be concerned with decay estimates of single coefficients $\langle f, \psi_\lambda \rangle$, but with the decay of sums of coefficients over several scales and all shears and translations. The frame property of the shearlet system, the C^2 -smoothness of f , and a crude counting argument of the cardinal of the essential indices λ will be enough to provide the needed approximation rate. The proof of this is similar to estimates of the decay of wavelet coefficients for C^2 smooth functions. In fact, shearlet and wavelet frames gives the same approximation decay rates in this case. Due to space limitation of this exposition, we will not go into the details of this estimate, but rather focus on the main part of the proof, *Case 2*.

For *Case 2* we need to estimate each coefficient $\langle f, \psi_\lambda \rangle$ individually and, in particular, how $|\langle f, \psi_\lambda \rangle|$ decays with scale j and shearing k . Without loss of generality we can assume that $f = f_0 + \chi_B f_1$ with $f_0 = 0$. We let then M denote the area of integration in $\langle f, \psi_\lambda \rangle$, that is,

$$M = \text{supp } \psi_\lambda \cap B.$$

Further, let \mathcal{L} be an affine hyperplane (in other and simpler words, a line in \mathbb{R}^2) that intersects M and thereby divides M into two sets M_t and M_l , see the sketch in Fig. 10. We thereby have that

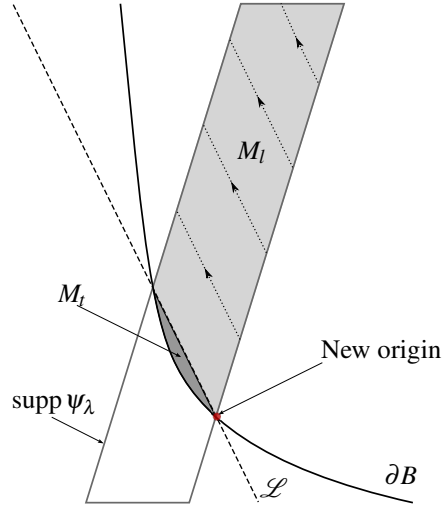
$$\langle f, \psi_\lambda \rangle = \langle \chi_M f, \psi_\lambda \rangle = \langle \chi_{M_t} f, \psi_\lambda \rangle + \langle \chi_{M_l} f, \psi_\lambda \rangle. \quad (26)$$

The hyperplane will be chosen in such way that the area of M_t is sufficiently small. In particular, $\text{area}(M_t)$ should be small enough so that the following estimate

$$|\langle \chi_{M_t} f, \psi_\lambda \rangle| \leq \|f\|_{L^\infty} \|\psi_\lambda\|_{L^\infty} \text{area}(M_t) \leq \mu 2^{3j/4} \text{area}(M_t) \quad (27)$$

do not violate (19). If the hyperplane \mathcal{L} is positioned as indicated in Fig. 10, it can indeed be shown by crudely estimating $\text{area}(M_t)$ that (27) does not violate estimate (19). We call estimates of this form, where we have restricted the integration to a small part M_t of M , *truncated* estimates. Hence, in the following we assume that (26) reduces to $\langle f, \psi_\lambda \rangle = \langle \chi_{M_l} f, \psi_\lambda \rangle$.

Fig. 10 Sketch of $\text{supp } \psi_\lambda$, M_l , M_t , and \mathcal{L} . The lines of integrations are shown.



For the term $\langle \chi_{M_l} f, \psi_\lambda \rangle$ we will have to integrate over a possibly much large part M_l of M . To handle this, we will use that ψ_λ only interacts with the discontinuity of $\chi_{M_l} f$ along a line inside M . This part of the estimate is called the *linearized* estimate, since the discontinuity curve in $\langle \chi_{M_l} f, \psi_\lambda \rangle$ has been reduced to a line. In $\langle \chi_{M_l} f, \psi_\lambda \rangle$ we are, of course, integrating over two variables, and we will as the inner integration always choose to integrate along lines parallel to the ‘singularity’ line \mathcal{L} , see Fig. 10. The important point here is that along these lines, the function f is C^2 -smooth without discontinuities on the entire interval of integration. This is exactly the reason for removing the M_t -part from M . Using the Fourier slice theorem we will

then turn the line integrations along \mathcal{L} in the spatial domain into line integrations in the frequency domain. The argumentation is as follows: Consider $g : \mathbb{R}^2 \rightarrow \mathbb{C}$ compactly supported and continuous, and let $p : \mathbb{R} \rightarrow \mathbb{C}$ be a projection of g onto, say, the x_2 axis, i.e., $p(x_1) = \int_{\mathbb{R}} g(x_1, x_2) dx_2$. This immediately implies that $\hat{p}(\xi_1) = \hat{g}(\xi_1, 0)$ which is a simplified version of the Fourier slice theorem. By an inverse Fourier transform, we then have

$$\int_{\mathbb{R}} g(x_1, x_2) dx_2 = p(x_1) = \int_{\mathbb{R}} \hat{g}(\xi_1, 0) e^{2\pi i x_1 \xi_1} d\xi_1, \quad (28)$$

and hence

$$\int_{\mathbb{R}} |g(x_1, x_2)| dx_2 = \int_{\mathbb{R}} |\hat{g}(\xi_1, 0)| d\xi_1. \quad (29)$$

The left-hand side of (29) corresponds to line integrations of g along vertical lines $x_1 = \text{constant}$. By applying shearing to the coordinates $x \in \mathbb{R}^2$, we can transform \mathcal{L} into a line of the form $\{x \in \mathbb{R}^2 : x_1 = \text{constant}\}$, whereby we can apply (29) directly.

We will make this idea more concrete in the proof of the following key estimate for linearized terms of the form $\langle \chi_{M_l} f, \psi_\lambda \rangle$. Since we assume the truncated estimate as negligible, this will in fact allow us to estimate $\langle f, \psi_\lambda \rangle$.

Theorem 9. *Let $\psi \in L^2(\mathbb{R}^2)$ be compactly supported, and assume that ψ satisfies the conditions in Setup 2. Further, let λ be such that $\text{supp } \psi_\lambda \cap \partial B \neq \emptyset$. Suppose that $f \in \mathcal{E}(\mathbb{R}^2)$ and that ∂B is linear on the support of ψ_λ in the sense*

$$\text{supp } \psi_\lambda \cap \partial B \subset \mathcal{L}$$

for some affine hyperplane \mathcal{L} of \mathbb{R}^2 . Then,

(i) if \mathcal{L} has normal vector $(-1, s)$ with $|s| \leq 3$,

$$|\langle f, \psi_\lambda \rangle| \lesssim \frac{2^{-3j/4}}{|k + 2^{j/2}s|^3},$$

(ii) if \mathcal{L} has normal vector $(-1, s)$ with $|s| \geq 3/2$,

$$|\langle f, \psi_\lambda \rangle| \lesssim 2^{-9j/4},$$

(iii) if \mathcal{L} has normal vector $(0, s)$ with $s \in \mathbb{R}$, then

$$|\langle f, \psi_\lambda \rangle| \lesssim 2^{-11j/4}.$$

Proof. Fix λ , and let $f \in \mathcal{E}(\mathbb{R}^2)$. We can without loss of generality assume that f is only nonzero on B .

Cases (i) and (ii). We first consider the cases (i) and (ii). In these cases, the hyperplane can be written as

$$\mathcal{L} = \{x \in \mathbb{R}^2 : \langle x - x_0, (-1, s) \rangle = 0\}$$

for some $x_0 \in \mathbb{R}^2$. We shear the hyperplane by S_{-s} for $s \in \mathbb{R}$ and obtain

$$\begin{aligned} S_{-s}\mathcal{L} &= \{x \in \mathbb{R}^2 : \langle S_s x - x_0, (-1, s) \rangle = 0\} \\ &= \{x \in \mathbb{R}^2 : \langle x - S_{-s}x_0, (S_s)^T(-1, s) \rangle = 0\} \\ &= \{x \in \mathbb{R}^2 : \langle x - S_{-s}x_0, (-1, 0) \rangle = 0\} \\ &= \{x = (x_1, x_2) \in \mathbb{R}^2 : x_1 = \hat{x}_1\}, \quad \text{where } \hat{x} = S_{-s}x_0, \end{aligned}$$

which is a line parallel to the x_2 -axis. Here the power of shearlets comes into play, since it will allow us to only consider line singularities parallel to the x_2 -axis. Of course, this requires that we also modify the shear parameter of the shearlet, that is, we will consider the right hand side of

$$\langle f, \psi_{j,k,m} \rangle = \langle f(S_s \cdot), \psi_{j,\hat{k},m} \rangle$$

with the new shear parameter $\hat{k} = k + 2^{j/2}s$. The integrand in $\langle f(S_s \cdot), \psi_{j,\hat{k},m} \rangle$ has the singularity plane exactly located on the line $x_1 = \hat{x}_1$, i.e., on $S_{-s}\mathcal{L}$.

To simplify the expression for the integration bounds, we will fix a new origin on $S_{-s}\mathcal{L}$, that is, on $x_1 = \hat{x}_1$; the x_2 coordinate of the new origin will be fixed in the next paragraph. Since f is only nonzero of B , the function f will be equal to zero on one side of $S_{-s}\mathcal{L}$, say, $x_1 < \hat{x}_1$. It therefore suffices to estimate

$$\langle f_0(S_s \cdot) \chi_\Omega, \psi_{j,\hat{k},m} \rangle$$

for $f_0 \in C^\beta(\mathbb{R}^2)$ and $\Omega = \mathbb{R}_+ \times \mathbb{R}$. Let us assume that $\hat{k} < 0$. The other case can be handled similarly.

Since ψ is compactly supported, there exists some $c > 0$ such that $\text{supp } \psi \subset [-c, c]^2$. By a rescaling argument, we can assume $c = 1$. Let

$$\mathcal{P}_{j,k} := \left\{ x \in \mathbb{R}^2 : |x_1 + 2^{-j/2}kx_2| \leq 2^{-j}, |x_2| \leq 2^{-j/2} \right\}, \quad (30)$$

With this notation we have $\text{supp } \psi_{j,k,0} \subset \mathcal{P}_{j,k}$. We say that the shearlet normal direction of the shearlet box $\mathcal{P}_{j,0}$ is $(1, 0)$, thus the shearlet normal of a sheared element $\psi_{j,k,m}$ associated with $\mathcal{P}_{j,k}$ is $(1, k/2^{j/2})$. Now, we fix our origin so that, relative to this new origin, it holds that

$$\text{supp } \psi_{j,\hat{k},m} \subset \mathcal{P}_{j,\hat{k}} + (2^{-j}, 0) =: \tilde{\mathcal{P}}_{j,k}.$$

Then one face of $\tilde{\mathcal{P}}_{j,k}$ intersects the origin.

Next, observe that the parallelogram $\tilde{\mathcal{P}}_{j,k}$ has sides $x_2 = \pm 2^{-j/2}$,

$$2^j x_1 + 2^{j/2} \hat{k} x_2 = 0, \text{ and}$$

$$2^j x_1 + 2^{j/2} \hat{k} x_2 = 2.$$

As it is only a matter of scaling, we replace the right hand side of the last equation with 1 for simplicity. Solving the two last equalities for x_2 gives the following lines:

$$\begin{aligned} L_1 : \quad x_2 &= -\frac{2^{j/2}}{\hat{k}}x_1, \text{ and} \\ L_2 : \quad x_2 &= -\frac{2^{j/2}}{\hat{k}}x_1 + \frac{2^{-j/2}}{\hat{k}}, \end{aligned}$$

We shows that

$$\left| \left\langle f_0(S_s \cdot) \chi_\Omega, \psi_{j,\hat{k},m} \right\rangle \right| \lesssim \left| \int_0^{K_1} \int_{L_2}^{L_1} f_0(S_s x) \psi_{j,\hat{k},m}(x) dx_2 dx_1, \right| \quad (31)$$

where the upper integration bound for x_1 is $K_1 = 2^{-j} - 2^{-j}\hat{k}$; this follows from solving L_2 for x_1 and using that $|x_2| \leq 2^{-j/2}$. We remark that the inner integration over x_2 is along lines parallel to the singularity line $\partial\Omega = \{0\} \times \mathbb{R}$; as mentioned, this allows us to better handle the singularity and will be used several times throughout this section.

We consider the one-dimensional Taylor expansion for $f_0(S_s \cdot)$ at each point $x = (x_1, x_2) \in L_2$ in the x_2 -direction:

$$f_0(S_s x) = a(x_1) + b(x_1) \left(x_2 + \frac{2^{j/2}}{\hat{k}} x_1 \right) + c(x_1, x_2) \left(x_2 + \frac{2^{j/2}}{\hat{k}} x_1 \right)^2,$$

where $a(x_1), b(x_1)$ and $c(x_1, x_2)$ are all bounded in absolute value by $C(1 + |s|)^2$. Using this Taylor expansion in (31) yields

$$\left| \left\langle f_0(S_s \cdot) \chi_\Omega, \psi_{j,\hat{k},m} \right\rangle \right| \lesssim (1 + |s|)^2 \left| \int_0^{K_1} \sum_{l=1}^3 I_l(x_1) dx_1 \right|, \quad (32)$$

where

$$I_1(x_1) = \left| \int_{L_1}^{L_2} \psi_{j,\hat{k},m}(x) dx_2 \right|, \quad (33)$$

$$I_2(x_1) = \left| \int_{L_1}^{L_2} (x_2 + K_2) \psi_{j,\hat{k},m}(x) dx_2 \right|, \quad (34)$$

$$I_3(x_1) = \left| \int_0^{-2^{-j/2}/\hat{k}} (x_2)^2 \psi_{j,\hat{k},m}(x_1, x_2 - K_2) dx_2 \right|, \quad (35)$$

and

$$K_2 = \frac{2^{j/2}}{\hat{k}} x_1.$$

We next estimate each integral $I_1 - I_3$ separately.

Integral I_1 . We first estimate $I_1(x_1)$. The Fourier slice theorem, see also (28), yields directly that

$$I_1(x_1) = \left| \int_{\mathbb{R}} \psi_{j,\hat{k},m}(x) dx_2 \right| = \left| \int_{\mathbb{R}^2} \hat{\psi}_{j,\hat{k},m}(\xi_1, 0) e^{2\pi i x_1 \xi_1} d\xi_1 \right|.$$

By the assumptions from Setup 2 we have, for all $\xi = (\xi_1, \xi_2, \xi_3) \in \mathbb{R}^2$,

$$|\hat{\psi}_{j,\hat{k},m}(\xi)| \lesssim 2^{-3j/4} |h(2^{-j}\xi_1)| \left(1 + \left| \frac{2^{-j/2}\xi_2}{2^{-j}\xi_1} + \hat{k} \right| \right)^{-\gamma}$$

for some $h \in L^1(\mathbb{R})$. Hence, we can continue our estimate of I_1 by

$$I_1(x_1) \lesssim \int_{\mathbb{R}} 2^{-3j/4} |h(2^{-j}\xi_1)| (1 + |\hat{k}|)^{-\gamma} d\xi_1,$$

and further, by a change of variables,

$$I_1(x_1) \lesssim \int_{\mathbb{R}} 2^{j/4} |h(\xi_1)| (1 + |\hat{k}|)^{-\gamma} d\xi_1 \lesssim 2^{j/4} (1 + |\hat{k}|)^{-\gamma}, \quad (36)$$

since $h \in L^1(\mathbb{R})$.

Integral I_2 . We start estimating $I_2(x_1)$ by

$$I_2(x_1) \leq \left| \int_{\mathbb{R}} x_2 \psi_{j,\hat{k},m}(x) dx_2 \right| + |K_2| \left| \int_{\mathbb{R}} \psi_{j,\hat{k},m}(x) dx_2 \right| =: S_1 + S_2.$$

Applying the Fourier slice theorem again and then utilizing the decay assumptions on $\hat{\psi}$ yields

$$\begin{aligned} S_1 &= \left| \int_{\mathbb{R}} x_2 \psi_{j,\hat{k},m}(x) dx_2 \right| \leq \left| \int_{\mathbb{R}} \left(\frac{\partial}{\partial \xi_2} \hat{\psi}_{j,\hat{k},m} \right) (\xi_1, 0) e^{2\pi i x_1 \xi_1} d\xi_1 \right| \\ &\lesssim \int_{\mathbb{R}} 2^{-j/2} 2^{-3j/4} |h(2^{-j}\xi_1)| (1 + |\hat{k}|)^{-\gamma} d\xi_1 \lesssim 2^{-j/4} (1 + |\hat{k}|)^{-\gamma}. \end{aligned}$$

Since $|x_1| \leq -\hat{k}_1/2^j$, we have $K_2 \leq 2^{-j/2}$. The following estimate of S_2 then follows directly from the estimate of I_1 :

$$S_2 \lesssim |K_2| 2^{j/4} (1 + |\hat{k}|)^{-\gamma} \lesssim 2^{-j/4} (1 + |\hat{k}|)^{-\gamma}.$$

From the two last estimate, we conclude that $I_2(x_1) \lesssim 2^{-j/4} (1 + |\hat{k}|)^{-\gamma}$.

Integral I_3 . Finally, we estimate $I_3(x_1)$ by

$$I_3(x_1) \leq \left| \int_0^{2^{-j/2}/\hat{k}} (x_2)^2 \|\psi_{j,\hat{k},m}\|_{L^\infty} dx_2 \right|$$

$$\lesssim 2^{3j/4} \left| \int_0^{-2^{-j/2}/\hat{k}} (x_2)^2 dx_2 \right| \lesssim 2^{-3j/4} |\hat{k}|^{-3}. \quad (37)$$

We see that I_2 decays faster than I_1 , hence we can leave I_2 out of our analysis. Applying (36) and (37) to (32), we obtain

$$\left| \langle f_0(S_{s^\cdot}) \chi_\Omega, \psi_{j,\hat{k},m} \rangle \right| \lesssim (1+|s|)^2 \left(\frac{2^{-3j/4}}{(1+|\hat{k}|)^{\gamma-1}} + \frac{2^{-7j/4}}{|\hat{k}|^2} \right). \quad (38)$$

Suppose that $s \leq 3$. Then (38) reduces to

$$\begin{aligned} |\langle f, \psi_{j,k,m} \rangle| &\lesssim \frac{2^{-3j/4}}{(1+|\hat{k}|)^{\gamma-1}} + \frac{2^{-7j/4}}{|\hat{k}|^2} \\ &\lesssim \frac{2^{-3j/4}}{(1+|\hat{k}|)^3}, \end{aligned}$$

since $\gamma \geq 4$. This proves (i).

On the other hand, if $s \geq 3/2$, then

$$|\langle f, \psi_{j,k,m} \rangle| \lesssim 2^{-9j/4}.$$

To see this, note that

$$\frac{2^{-\frac{3}{4}j}}{(1+|k+s2^{j/2}|)^3} = \frac{2^{-\frac{9}{4}j}}{(2^{-j/2}+|k/2^{-j/2}+s|)^3} \leq \frac{2^{-\frac{9}{4}j}}{|k/2^{j/2}+s|^3}$$

and

$$|k/2^{j/2}+s| \geq |s| - |k/2^{j/2}| \geq 1/2 - 2^{-j/2} \geq 1/4$$

for sufficiently large $j \geq 0$, since $|k| \leq \lceil 2^{j/2} \rceil \leq 2^{j/2} + 1$, and (ii) is proven.

Case (iii). Finally, we need to consider the case (iii), in which the normal vector of the hyperplane \mathcal{L} is of the form $(0, s)$ for $s \in \mathbb{R}$. For this, let $\tilde{\Omega} = \{x \in \mathbb{R}^2 : x_2 \geq 0\}$. As in the first part of the proof, it suffices to consider coefficients of the form $\langle \chi_{\tilde{\Omega}} f_0, \psi_{j,k,m} \rangle$, where $\text{supp } \psi_{j,k,m} \subset \mathcal{P}_{j,k} - (2^{-j}, 0) = \tilde{\mathcal{P}}_{j,k}$ with respect to some new origin. As before, the boundary of $\tilde{\mathcal{P}}_{j,k}$ intersects the origin. By the assumptions in Setup 2, we have that

$$\left(\frac{\partial}{\partial \xi_1} \right)^\ell \hat{\psi}(0, \xi_2) = 0 \quad \text{for } \ell = 0, 1,$$

which implies that

$$\int_{\mathbb{R}} x_1^\ell \psi(x) dx_1 = 0 \quad \text{for all } x_2 \in \mathbb{R} \text{ and } \ell = 0, 1.$$

Therefore, we have

$$\int_{\mathbb{R}} x_1^\ell \psi(S_k x) dx_1 = 0 \quad \text{for all } x_2 \in \mathbb{R}, k \in \mathbb{R}, \text{ and } \ell = 0, 1, \quad (39)$$

since a shearing operation S_k preserves vanishing moments along the x_1 axis. Now, we employ Taylor expansion of f_0 in the x_1 -direction (that is, again along the singularity line $\partial\tilde{Q}$). By (39) everything but the last term in the Taylor expansion disappears, and we obtain

$$\begin{aligned} |\langle \chi_{\tilde{Q}} f_0, \psi_{j,k,m} \rangle| &\lesssim 2^{3j/4} \int_0^{2^{-j/2}} \int_{-2^{-j}}^{2^{-j}} (x_1)^2 dx_1 dx_2 \\ &\lesssim 2^{3j/4} 2^{-j/2} 2^{-3j} = 2^{-11j/4}, \end{aligned}$$

which proves claim (iii). \square

We are now ready show the estimates (21) and (22), which by Lem. 2(ii) completes the proof of Thm. 5.

For $j \geq 0$, fix $Q \in \mathcal{Q}_j^0$, where $\mathcal{Q}_j^0 \subset \mathcal{Q}_j$ is the collection of dyadic squares that intersects \mathcal{L} . We then have the following counting estimate:

$$\#|M_{j,k,Q}| \lesssim |k + 2^{j/2}s| + 1 \quad (40)$$

for each $|k| \leq \lceil 2^{j/2} \rceil$, where

$$M_{j,k,Q} := \{m \in \mathbb{Z}^2 : |\text{supp } \psi_{j,k,m} \cap \mathcal{L} \cap Q| \neq 0\}$$

To see this claim, note that for a fixed j and k we need to count the number of translates $m \in \mathbb{Z}^2$ for which the support of $\psi_{j,k,m}$ intersects the discontinuity line $\mathcal{L} : x_1 = sx_2 + b$, $b \in \mathbb{R}$, inside Q . Without loss of generality, we can assume that $Q = [0, 2^{-j/2}]^2$, $b = 0$, and $\text{supp } \psi_{j,k,0} \subset C \cdot \mathcal{P}_{j,k}$, where $\mathcal{P}_{j,k}$ is defined as in (30). The shearlet $\psi_{j,k,m}$ will therefore be concentrated around the line $\mathcal{S}_m : x_1 = -\frac{k}{2^{j/2}}x_2 + 2^{-j}m_1 + 2^{-j/2}m_2$, see also Fig. 9b. We will count the number of $m = (m_1, m_2) \in \mathbb{Z}^2$ for which these two lines intersect inside Q since this number, up to multiplication with a constant independent of the scale j , will be equal to $\#|M_{j,k,Q}|$.

First note that since the size of Q is $2^{-j/2} \times 2^{-j/2}$, only a finite number of m_2 translates can make $\mathcal{S}_m \cap \mathcal{L} \cap Q \neq \emptyset$ whenever $m_1 \in \mathbb{Z}$ is fixed. For a fixed $m_2 \in \mathbb{Z}$, we then estimate the number of relevant m_1 translates. Equating the x_1 coordinates in \mathcal{L} and \mathcal{S}_m yields

$$\left(\frac{k}{2^{j/2}} + s\right)x_2 = 2^{-j}m_1 + 2^{-j/2}m_2.$$

Without loss of generality, we take $m_2 = 0$ which then leads to

$$2^{-j}|m_1| \leq 2^{-j/2} |k + 2^{j/2}s| |x_2| \leq 2^{-j} |k + 2^{j/2}s|,$$

hence $|m_1| \leq |k + 2^{j/2}s|$. This completes the proof of the claim.

For $\varepsilon > 0$, we will consider the shearlet coefficients larger than ε in absolute value. Thus, we define:

$$M_{j,k,Q}(\varepsilon) = \{m \in M_{j,k,Q} : |\langle f, \psi_{j,k,m} \rangle| > \varepsilon\},$$

where $Q \in \mathcal{Q}_j^0$. Since the discontinuity line \mathcal{L} has finite length in $[0, 1]^2$, we have the estimate $\#\mathcal{Q}_j^0 \lesssim 2^{j/2}$. Assume \mathcal{L} has normal vector $(-1, s)$ with $|s| \leq 3$. Then, by Thm. 9(i), $|\langle f, \psi_{j,k,m} \rangle| > \varepsilon$ implies that

$$|k + 2^{j/2}s| \leq \varepsilon^{-1/3} 2^{-j/4}. \quad (41)$$

By Lem. 2(i) and the estimates (40) and (41), we have that

$$\begin{aligned} \#|\Lambda(\varepsilon)| &\lesssim \sum_{j=0}^{\frac{4}{3}\log_2(\varepsilon^{-1})+C} \sum_{Q \in \mathcal{Q}_j^0} \sum_{\{\hat{k}: |\hat{k}| \leq \varepsilon^{-1/3} 2^{-j/4}\}} \#|M_{j,k,Q}(\varepsilon)| \\ &\lesssim \sum_{j=0}^{\frac{4}{3}\log_2(\varepsilon^{-1})+C} \sum_{Q \in \mathcal{Q}_j^0} \sum_{\{\hat{k}: |\hat{k}| \leq \varepsilon^{-1/3} 2^{-j/4}\}} (|\hat{k}| + 1) \\ &\lesssim \sum_{j=0}^{\frac{4}{3}\log_2(\varepsilon^{-1})+C} \#\mathcal{Q}_j^0 (\varepsilon^{-2/3} 2^{-j/2}) \\ &\lesssim \varepsilon^{-2/3} \sum_{j=0}^{\frac{4}{3}\log_2(\varepsilon^{-1})+C} 1 \lesssim \varepsilon^{-2/3} \log_2(\varepsilon^{-1}), \end{aligned}$$

where, as usual, $\hat{k} = k + s2^{j/2}$. By Lem. 2(ii), this leads to the sought estimates.

On the other hand, if \mathcal{L} has normal vector $(0, 1)$ or $(-1, s)$ with $|s| \geq 3$, then $|\langle f, \psi_\lambda \rangle| > \varepsilon$ implies that

$$j \leq \frac{4}{9} \log_2(\varepsilon^{-1}),$$

which follows by assertions (ii) and (iii) in Thm. 9. Hence, we have

$$\#|\Lambda(\varepsilon)| \lesssim \sum_{j=0}^{\frac{4}{9}\log_2(\varepsilon^{-1})} \sum_k \sum_{Q \in \mathcal{Q}_j^0} \#|M_{j,k,Q}(\varepsilon)|.$$

Note that $\#|M_{j,k,Q}| \lesssim 2^{j/2}$, since $\#\{m \in \mathbb{Z}^2 : |\text{supp } \psi_\lambda \cap Q| \neq 0\} \lesssim 2^{j/2}$ for each $Q \in \mathcal{Q}_j$, and that the number of shear parameters k for each scale parameter $j \geq 0$ is bounded by $C2^{j/2}$. Therefore,

$$\#|\Lambda(\varepsilon)| \lesssim \sum_{j=0}^{\frac{4}{9}\log_2(\varepsilon^{-1})} 2^{j/2} 2^{j/2} 2^{j/2} = \sum_{j=0}^{\frac{4}{9}\log_2(\varepsilon^{-1})} 2^{3j/2} \lesssim 2^{\frac{4}{9} \cdot \frac{3}{2} \cdot \log_2(\varepsilon^{-1})} \lesssim \varepsilon^{-2/3}.$$

This implies our sought estimate (21) which, together with the estimate for $|s| \leq 3$, completes the proof of Thm. 5 for $L = 1$ under Setup 2. \square

5.1.7 The Case $L \neq 1$

We now turn to the extended class of cartoon-like images $\mathcal{E}_L^2(\mathbb{R}^2)$ with $L \neq 1$, i.e., in which the singularity curve is only required to be piecewise C^2 . We say that $p \in \mathbb{R}^2$ is a corner point if ∂B is not C^2 smooth in p . The main focus here will be to investigate shearlets that interact with one of the L corner points. We will argue that Thm. 5 also holds in this extended setting. The rest of the proof, that is, for shearlets *not* interacting with corner points, is of course identical to that presented in Sect. 5.1.5 and 5.1.6.

In the compactly supported case one can simply count the number of shearlets interacting with a corner point at a given scale. Using Lem. 2(i), one then arrives at the sought estimate. On the other hand, for the band-limited case one needs to measure the sparsity of the shearlet coefficients for f localized to each dyadic square. We present the details in the remainder of this section.

Band-limited Shearlets In this case, it is sufficient to consider a dyadic square $Q \in \mathcal{Q}_j^0$ with $j \geq 0$ such that Q contains a singular point of edge curve. Especially, we may assume that j is sufficiently large so that the dyadic square $Q \in \mathcal{Q}_j^0$ contains a single corner point of ∂B . The following theorem analyzes the sparsity of the shearlet coefficients for such a dyadic square $Q \in \mathcal{Q}_j^0$.

Theorem 10. *Let $f \in \mathcal{E}_L^2(\mathbb{R}^2)$ and $Q \in \mathcal{Q}_j^0$ with $j \geq 0$ be a dyadic square containing a singular point of the edge curve. The sequence of shearlet coefficients $\{d_\lambda := \langle f_Q, \psi_\lambda \rangle : \lambda \in \Lambda_j\}$ obeys*

$$\left\| (d_\lambda)_{\lambda \in \Lambda_j} \right\|_{w\ell^{2/3}} \leq C.$$

The proof of Thm. 10 is based on a proof of an analog result for curvelets [4]. Although the proof in [4] considers only curvelet coefficients, essentially the same arguments, with modifications to the shearlet setting, can be applied to show Thm. 10.

Finally, we note that the number of dyadic squares $Q \in \mathcal{Q}_j^0$ containing a singular point of ∂B is bounded by a constant not depending on j ; one could, e.g., take L as this constant. Therefore, applying Thm. 10 and repeating the arguments in Sect. 5.1.5 completes the proof of Thm. 5 for $L \neq 1$ for Setup 1.

Compactly Supported Shearlets In this case, it is sufficient to consider the following two cases.

Case 1. The shearlet ψ_λ intersects a corner point, in which two C^2 curves ∂B_0 and ∂B_1 , say, meet (see Fig. 11a).

Case 2. The shearlet ψ_λ intersects two edge curves ∂B_0 and ∂B_1 , say, simultaneously, but it does not intersect a corner point (see Fig. 11b).

We aim to show that $\#\Lambda(\epsilon) \lesssim \epsilon^{-\frac{2}{3}}$ in both cases. By Lem. 2, this will be sufficient.

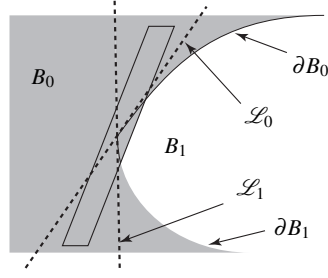


Fig. 11a A shearlet ψ_λ intersecting a corner point, in which two edge curves ∂B_0 and ∂B_1 meet. \mathcal{L}_0 and \mathcal{L}_1 are tangents to the edge curves ∂B_0 and ∂B_1 in this corner point.

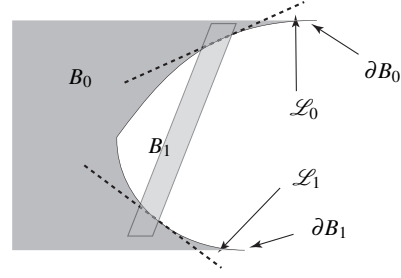


Fig. 11b A shearlet ψ_λ intersecting two edge curves ∂B_0 and ∂B_1 which are part of the boundary of sets B_0 and B_1 . \mathcal{L}_0 and \mathcal{L}_1 are tangents to the edge curves ∂B_0 and ∂B_1 in points contained in the support of ψ_λ .

Case 1. Since there exist only finitely many corner points with total number not depending on scale $j \geq 0$ and the number of shearlets ψ_λ intersecting each of corner points is bounded by $C2^{j/2}$, we have

$$\#|\Lambda(\varepsilon)| \lesssim \sum_{j=0}^{\frac{4}{3} \log_2(\varepsilon^{-1})} 2^{j/2} \lesssim \varepsilon^{-\frac{2}{3}}.$$

Case 2. As illustrated in Fig. 11b, we can write the function f as

$$f_0 \chi_{B_0} + f_1 \chi_{B_1} = (f_0 - f_1) \chi_{B_0} + f_1 \quad \text{in } Q,$$

where $f_0, f_1 \in C^2([0, 1]^2)$ and B_0, B_1 are two disjoint subsets of $[0, 1]^2$. As we indicated before, the rate for optimal sparse approximation is achieved for the smooth function f_1 . Thus, it is sufficient to consider $f := g_0 \chi_{B_0}$ with $g_0 = f_0 - f_1 \in C^2([0, 1]^2)$. By a *truncated* estimate, we can replace two boundary curves ∂B_0 and ∂B_1 by hyperplanes of the form

$$\mathcal{L}_i = \{x \in \mathbb{R}^2 : \langle x - x_0, (-1, s_i) \rangle = 0\} \quad \text{for } i = 0, 1.$$

In the sequel, we assume $\max_{i=0,1} |s_i| \leq 3$ and mention that the other cases can be handled similarly. Next define

$$M_{j,k,Q}^i = \{m \in \mathbb{Z}^2 : |\text{supp } \psi_{j,k,m} \cap \mathcal{L}_i \cap Q| \neq 0\} \quad \text{for } i = 0, 1,$$

for each $Q \in \tilde{\mathcal{Q}}_j^0$, where $\tilde{\mathcal{Q}}_j^0$ denotes the dyadic squares containing the two distinct boundary curves. By an estimate similar to (40), we obtain

$$\# \left| M_{j,k,Q}^0 \cap M_{j,k,Q}^1 \right| \lesssim \min_{i=0,1} (|k + 2^{j/2} s_i| + 1). \quad (42)$$

Applying Thm. 9(i) to each of the hyperplanes \mathcal{L}_0 and \mathcal{L}_1 , we also have

$$|\langle f, \psi_{j,k,m} \rangle| \leq C \cdot \max_{i=0,1} \left\{ \frac{2^{-\frac{3}{4}j}}{|2^{j/2}s_i + k|^3} \right\}. \quad (43)$$

Let $\hat{k}_i = k + 2^{j/2}s_i$ for $i = 0, 1$. Without loss of generality, we may assume that $\hat{k}_0 \leq \hat{k}_1$. Then, (42) and (43) imply that

$$\# |M_{j,Q}^0 \cap M_{j,Q}^1| \lesssim |\hat{k}_0| + 1 \quad (44)$$

and

$$|\langle f, \psi_{j,k,m} \rangle| \lesssim \frac{2^{-\frac{3}{4}j}}{|\hat{k}_0|^3}. \quad (45)$$

Using (44) and (45), we now estimate $\#|\Lambda(\varepsilon)|$ as follows:

$$\begin{aligned} \#|\Lambda(\varepsilon)| &\lesssim \sum_{j=0}^{\frac{4}{3}\log_2(\varepsilon^{-1})+C} \sum_{Q \in \tilde{\mathcal{Q}}_j^0} \sum_{k_0} (1 + |\hat{k}_0|) \\ &\lesssim \sum_{j=0}^{\frac{4}{3}\log_2(\varepsilon^{-1})+C} \#|\tilde{\mathcal{Q}}_j^0| (\varepsilon^{-2/3} 2^{-j/2}) \lesssim \varepsilon^{-2/3}. \end{aligned}$$

Note that $\#|\tilde{\mathcal{Q}}_j^0| \leq C$ since the number of $Q \in \mathcal{Q}_j$ containing two distinct boundary curves ∂B_0 and ∂B_1 is bounded by a constant independent of j . The result is proved. \square

5.2 Optimal Sparse Approximations in 3D

When passing from 2D to 3D, the complexity of anisotropic structures changes significantly. In particular, as opposed to the two dimensional setting, geometric structures of discontinuities for piecewise smooth 3D functions consist of two morphologically different types of structure, namely surfaces and curves. Moreover, as we saw in Sect. 5.1, the analysis of sparse approximations in 2D heavily depends on reducing the analysis to affine subspaces of \mathbb{R}^2 . Clearly, these subspaces always have dimension one in 2D. In dimension three, however, we have subspaces of dimension one and two, and therefore the analysis needs to be performed on subspaces of the ‘correct’ dimension.

This issue manifests itself when performing the analysis for band-limited shearlets, since one needs to replace the Radon transform used in 2D with a so-called X-ray transform. For compactly supported shearlets, one needs to perform the analysis on carefully chosen hyperplanes of dimension two. This will allow for using estimates from the two dimensional setting in a slice by slice manner.

As in the two dimensional setting, analyzing the decay of individual shearlet coefficients $\langle f, \psi_\lambda \rangle$ can be used to show optimal sparsity for compactly supported shearlets while the sparsity of the sequence of shearlet coefficients with respect to the weak ℓ^p quasi norm should be analyzed for band-limited shearlets.

5.2.1 A Heuristic Analysis

As in the heuristic analysis for the 2D situation debated in Sect. 5.1.1, we can again split the proof into similar three cases as shown in Fig. 12.

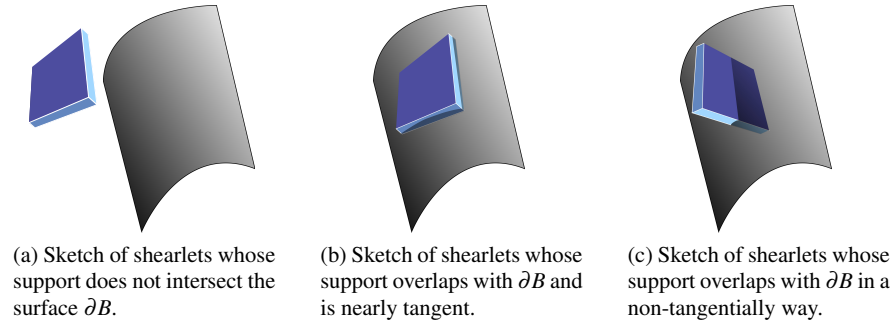


Fig. 12 The three types of shearlets $\psi_{j,k,m}$ and boundary ∂B interactions considered in the heuristic 3D analysis. Note that only a section of ∂B is shown.

Only case (b) differs significantly from the 2D setting, so we restrict our attention to that case.

For case (b) there are at most $O(2^j)$ coefficients at scale $j > 0$, since the plate-like elements are of size $2^{-j/2}$ times $2^{-j/2}$ (and ‘thickness’ 2^{-j}). By Hölder’s inequality, we see that

$$|\langle f, \psi_{j,k,m} \rangle| \leq \|f\|_{L^\infty} \|\psi_{j,k,m}\|_{L^1} \leq C_1 2^{-j} \|\psi\|_{L^1} \leq C_2 \cdot 2^{-j}$$

for some constants $C_1, C_2 > 0$. Hence, we have $O(2^j)$ coefficients bounded by $C_2 \cdot 2^{-j}$.

Assuming the coefficients in case (a) and (c) to be negligible, the n th largest shearlet coefficient c_n^* is therefore bounded by

$$|c_n^*| \leq C \cdot n^{-1},$$

which in turn implies

$$\sum_{n>N} |c_n^*|^2 \leq \sum_{n>N} C \cdot n^{-2} \leq C \cdot \int_N^\infty x^{-2} dx \leq C \cdot N^{-1}.$$

Hence, we meet the optimal rates (7) and (8) from Dfn. 1. This, at least heuristically, shows that shearlets provide optimally sparse approximations of 3D cartoon-like images.

5.2.2 Main Result

The hypotheses needed for the band-limited case, stated in Setup 3, are a straightforward generalization of Setup 1 in the two-dimensional setting.

Setup 3. The generators $\phi, \psi, \tilde{\psi}, \check{\psi} \in L^2(\mathbb{R}^3)$ are band-limited and C^∞ in the frequency domain. Furthermore, the shearlet system $SH(\phi, \psi, \tilde{\psi}, \check{\psi}; c)$ forms a frame for $L^2(\mathbb{R}^3)$ (cf. the construction in Sect. 4.2).

For the compactly supported generators we will also use hypotheses in the spirit of Setup 2, but with slightly stronger and more sophisticated assumption on vanishing moment property of the generators i.e., $\delta > 8$ and $\gamma \geq 4$.

Setup 4. The generators $\phi, \psi, \tilde{\psi}, \check{\psi} \in L^2(\mathbb{R}^3)$ are compactly supported, and the shearlet system $SH(\phi, \psi, \tilde{\psi}, \check{\psi}; c)$ forms a frame for $L^2(\mathbb{R}^3)$. Furthermore, the function ψ satisfies, for all $\xi = (\xi_1, \xi_2, \xi_3) \in \mathbb{R}^3$,

- (i) $|\hat{\psi}(\xi)| \leq C \cdot \min\{1, |\xi_1|^\delta\} \min\{1, |\xi_1|^{-\gamma}\} \min\{1, |\xi_2|^{-\gamma}\} \min\{1, |\xi_3|^{-\gamma}\},$
and
- (ii) $\left| \frac{\partial}{\partial \xi_i} \hat{\psi}(\xi) \right| \leq |h(\xi_1)| \left(1 + \frac{|\xi_2|}{|\xi_1|}\right)^{-\gamma} \left(1 + \frac{|\xi_3|}{|\xi_1|}\right)^{-\gamma},$

for $i = 2, 3$, where $\delta > 8$, $\gamma \geq 4$, $h \in L^1(\mathbb{R})$, and C a constant, and $\tilde{\psi}$ and $\check{\psi}$ satisfy analogous conditions with the obvious change of coordinates (cf. the construction in Sect. 4.3).

The main result can now be stated as follows.

Theorem 11 ([11, 15]). Assume Setup 3 or 4. Let $L = 1$. For any $v > 0$ and $\mu > 0$, the shearlet frame $SH(\phi, \psi, \tilde{\psi}, \check{\psi}; c)$ provides optimally sparse approximations of functions $f \in \mathcal{E}_L^2(\mathbb{R}^3)$ in the sense of Dfn. 1, i.e.,

$$\|f - f_N\|_{L^2}^2 \lesssim N^{-1}(\log N)^2, \quad \text{as } N \rightarrow \infty,$$

and

$$|c_n^*| \lesssim n^{-1}(\log n), \quad \text{as } n \rightarrow \infty,$$

where $c = \{ \langle f, \hat{\psi}_\lambda \rangle : \lambda \in \Lambda, \hat{\psi} = \psi, \hat{\psi} = \tilde{\psi}, \text{ or } \hat{\psi} = \check{\psi} \}$ and $c^* = (c_n^*)_{n \in \mathbb{N}}$ is a decreasing (in modulus) rearrangement of c .

We now give a sketch of proof for this theorem, and refer to [11, 15] for detailed proofs.

5.2.3 Sketch of Proof of Theorem 11

Band-limited Shearlets The proof of Thm. 11 for band-limited shearlets follows the same steps as discussed in Sect. 5.1.5 for the 2D case. To indicate the main steps, we will use the same notation as for the 2D proof with the straightforward extension to 3D.

Similar to Thm. 6 and 7, one can prove the following results on the sparsity of the shearlets coefficients for each dyadic square $Q \in \mathcal{Q}_j$.

Theorem 12 ([11]). *Let $f \in \mathcal{E}^2(\mathbb{R}^3)$. $Q \in \mathcal{Q}_j^0$, with $j \geq 0$ fixed, the sequence of shearlet coefficients $\{d_\lambda := \langle f_Q, \psi_\lambda \rangle : \lambda \in \Lambda_j\}$ obeys*

$$\|(d_\lambda)_{\lambda \in \Lambda_j}\|_{w\ell^1} \lesssim 2^{-2j}.$$

Theorem 13 ([11]). *Let $f \in \mathcal{E}^2(\mathbb{R}^3)$. For $Q \in \mathcal{Q}_j^1$, with $j \geq 0$ fixed, the sequence of shearlet coefficients $\{d_\lambda := \langle f_Q, \psi_\lambda \rangle : \lambda \in \Lambda_j\}$ obeys*

$$\|(d_\lambda)_{\lambda \in \Lambda_j}\|_{\ell^1} \lesssim 2^{-4j}.$$

The proofs of Thm. 12 and 13 follow the same principles as the proofs of the analog results in 2D, Thm. 6 and 7, with one important difference: In the proof of Thm. 6 and 7 the Radon transform (cf. (28)) is used to deduce estimates for the integral of edge-curve fragments. In 3D one needs to use a different transform, namely the so-called X-ray transform, which maps a function on \mathbb{R}^3 into the sets of its line integrals. The X-ray transform is then used to deduce estimates for the integral of the surface fragments. We refer to [11] for a detailed exposition.

As a consequence of Thm. 12 and 13, we have the following result.

Theorem 14 ([11]). *Suppose $f \in \mathcal{E}^2(\mathbb{R}^3)$. Then, for $j \geq 0$, the sequence of the shearlet coefficients $\{c_\lambda := \langle f, \psi_\lambda \rangle : \lambda \in \Lambda_j\}$ obeys*

$$\|(c_\lambda)_{\lambda \in \Lambda_j}\|_{w\ell^1} \lesssim 1.$$

Proof. The result follows by the same arguments used in the proof of Thm. 8. \square

By Thm. 14, we can now prove Thm. 11 for the band-limited setup and for $f \in \mathcal{E}_L^2(\mathbb{R}^3)$ with $L = 1$. The proof is very similar to the proof of Thm. 5 in Sect. 5.1.5, wherefore we will not repeat it.

Compactly Supported Shearlets In this section we will consider the key estimates for the linearized term for compactly supported shearlets in 3D. This is an extension of Thm. 9 to the three-dimensional setting. Hence, we will assume that the discontinuity surface is a plane, and consider the decay of the shearlet coefficients of shearlets interacting with such a discontinuity.

Theorem 15 ([15]). *Let $\psi \in L^2(\mathbb{R}^3)$ be compactly supported, and assume that ψ satisfies the conditions in Setup 4. Further, let λ be such that $\text{supp } \psi_\lambda \cap \partial B \neq \emptyset$. Suppose that $f \in \mathcal{E}^2(\mathbb{R}^3)$ and that ∂B is linear on the support of ψ_λ in the sense that*

$$\text{supp } \psi_\lambda \cap \partial B \subset \mathcal{H}$$

for some affine hyperplane \mathcal{H} of \mathbb{R}^3 . Then,

(i) *if \mathcal{H} has normal vector $(-1, s_1, s_2)$ with $s_1 \leq 3$ and $s_2 \leq 3$,*

$$|\langle f, \psi_\lambda \rangle| \lesssim \min_{i=1,2} \left\{ \frac{2^{-j}}{|k_i + 2^{j/2}s_i|^3} \right\},$$

(ii) *if \mathcal{H} has normal vector $(-1, s_1, s_2)$ with $s_1 \geq 3/2$ or $s_2 \geq 3/2$,*

$$|\langle f, \psi_\lambda \rangle| \lesssim 2^{-5j/2},$$

(iii) *if \mathcal{H} has normal vector $(0, s_1, s_2)$ with $s_1, s_2 \in \mathbb{R}$, then*

$$|\langle f, \psi_\lambda \rangle| \lesssim 2^{-3j},$$

Proof. Fix λ , and let $f \in \mathcal{E}^2(\mathbb{R}^3)$. We first consider the case (ii) and assume $s_1 \geq 3/2$. The hyperplane can be written as

$$\mathcal{H} = \{x \in \mathbb{R}^3 : \langle x - x_0, (-1, s_1, s_2) \rangle = 0\}$$

for some $x_0 \in \mathbb{R}^3$. For $\hat{x}_3 \in \mathbb{R}$, we consider the restriction of \mathcal{H} to the slice $x_3 = \hat{x}_3$. This is clearly a line of the form

$$\mathcal{L} = \{x = (x_1, x_2) \in \mathbb{R}^2 : \langle x - x'_0, (-1, s_1) \rangle = 0\}$$

for some $x'_0 \in \mathbb{R}^2$, hence we have reduced the singularity to a line singularity, which was already considered in Thm. 9. We apply now Thm. 9 to each on slice, and we obtain

$$|\langle f, \psi_\lambda \rangle| \lesssim 2^{j/4} 2^{-9j/4} 2^{-j/2} = 2^{-5j/2}.$$

The first term $2^{j/4}$ in the estimate above is due to the different normalization factor used for shearlets in 2D and 3D, the second term is the conclusion from Thm. 9, and the third is the length of the support of ψ_λ in the direction of x_3 . The case $s_2 \geq 3/2$ can be handled similarly with restrictions to slices $x_2 = \hat{x}_2$ for $\hat{x}_2 \in \mathbb{R}$. This completes the proof of case (ii).

The other two cases, i.e., case (i) and (ii), are proved using the same slice by slice technique and Thm. 9. \square

Neglecting truncated estimates, Thm. 15 can be used to prove the optimal sparsity result in Thm. 11. The argument is similar to the one in Sect. 5.1.6 and will not be repeated here. Let us simply argue that the decay rate $|\langle f, \psi_\lambda \rangle| \lesssim 2^{-5j/2}$ from Thm. 15(ii) is what is needed in the case $s_i \geq 3/2$. It is easy to see that in 3D an

estimate of the form

$$\#\Lambda(\varepsilon) \lesssim \varepsilon^{-1}.$$

will guarantee optimal sparsity. Since we in the estimate $|\langle f, \psi_\lambda \rangle| \lesssim 2^{-5j/2}$ have no control of the shearing parameter $k = (k_1, k_2)$, we have to use a crude counting estimate, where we include all shears at a given scale j , namely $2^{j/2} \cdot 2^{j/2} = 2^j$. Since the number of dyadic boxes Q where ∂B intersects the support of f is of order $2^{3j/2}$, we arrive at

$$\#\Lambda(\varepsilon) \lesssim \sum_{j=0}^{\frac{2}{5} \log_2(\varepsilon^{-1})} 2^{5j/2} \asymp \varepsilon^{-1}.$$

5.2.4 Some Extensions

Paralleling the two-dimensional setting (see Sect. 5.1.7), we can extend the optimality result in Thm. 11 to the cartoon-like image class $\mathcal{E}_L^2(\mathbb{R}^3)$ for $L \in \mathbb{N}$, in which the discontinuity surface ∂B is allowed to be *piecewise* C^2 smooth.

Moreover, the requirement that the ‘edge’ ∂B is piecewise C^2 might be too restrictive in some applications. Therefore, in [15], the cartoon-like image model class was enlarged to allow less regular images, where ∂B is piecewise C^α smooth for $1 < \alpha \leq 2$, and not necessarily a C^2 . This class $\mathcal{E}_{\alpha,L}^\beta(\mathbb{R}^3)$ was introduced in Sect. 2 consisting of *generalized* cartoon-like images having C^β smoothness apart from a piecewise C^α discontinuity curve. The sparsity results presented above in Thm. 11 can be extended to this generalized model class for compactly supported shearlets with a scaling matrix dependent on α . The optimal approximation error rate, as usual measured in $\|f - f_N\|_{L^2}^2$, for this generalized model is $N^{-\alpha/2}$; compare this to N^{-1} for the case $\alpha = 2$ considered throughout this chapter. For brevity we will not go into details of this, but mention the approximation error rate obtained by shearlet frames is slightly worse than in the $\alpha = \beta = 2$ case, since the error rate is not only a poly-log factor away from the optimal rate, but a small polynomial factor; and we refer to [15] the precise statement and proof.

5.2.5 Surprising Observations

Capturing anisotropic phenomenon in 3D is somewhat different from capturing anisotropic features in 2D as discussed in Sect. 1.3. While in 2D we ‘only’ have to handle curves, in 3D a more complex situation can occur since we find two geometrically very different anisotropic structures: curves and surfaces. Curves are clearly one-dimensional anisotropic features and surfaces two-dimensional features. Since our 3D shearlet elements are plate-like in spatial domain by construction, one could think that these 3D shearlet systems would *only* be able to efficiently capture two-dimensional anisotropic structures, and *not* one-dimensional structures. Nonetheless, surprisingly, as we have discussed in Sect. 5.2.4, these 3D shearlet systems

still perform optimally when representing and analyzing 3D data $\mathcal{E}_L^2(\mathbb{R}^3)$ that contain *both* curve and surface singularities (see e.g., Fig. 2).

Acknowledgements The first author acknowledges partial support by Deutsche Forschungsgemeinschaft (DFG) Grant KU 1446/14, and the first and third author acknowledge support by DFG Grant SPP-1324 KU 1446/13.

References

1. Introduction of this book!
2. Coorbit chapter of this book!
3. ShearLab chapter of this book!
4. E. J. Candès and D. L. Donoho, *New tight frames of curvelets and optimal representations of objects with piecewise C^2 singularities*, Comm. Pure and Appl. Math. **56** (2004), 216–266.
5. I. Daubechies, *Ten Lectures on Wavelets*, SIAM, Philadelphia, 1992.
6. R. A. DeVore, G. G. Lorentz, *Constructive Approximation*, Springer, Berlin, 1993.
7. M. N. Do and M. Vetterli, *The contourlet transform: an efficient directional multiresolution image representation*, IEEE Trans. Image Process. **14** (2005), 2091–2106.
8. D. L. Donoho, *Sparse components of images and optimal atomic decomposition*, Constr. Approx. **17** (2001), 353–382.
9. D. L. Donoho, *Wedgelets: nearly minimax estimation of edges*, Ann. Statist. **27** (1999), 859–897.
10. K. Guo and D. Labate, *Optimally sparse multidimensional representation using shearlets*, SIAM J. Math. Anal. **39** (2007), 298–318.
11. K. Guo and D. Labate, *Optimally sparse representations of 3D data with C^2 surface singularities using Parseval frames of shearlets*, preprint.
12. A. C. Kak and Malcolm Slaney, *Principles of Computerized Tomographic Imaging*, IEEE Press, 1988.
13. P. Kittipoom, G. Kutyniok, and W.-Q Lim, *Construction of compactly supported shearlet frames*, preprint.
14. S. Kuratsubo, *On pointwise convergence of Fourier series of the indicator function of D dimensional ball*, J. Fourier Anal. Appl. **16** (2010), 52–59.
15. G. Kutyniok, J. Lemvig, and W.-Q Lim, *Compactly supported shearlet frames and optimally sparse approximations of functions in $L^2(\mathbb{R}^3)$ with piecewise C^α singularities*, preprint.
16. G. Kutyniok, J. Lemvig, and W.-Q Lim, *Compactly supported shearlets*, in Approximation Theory XIII (San Antonio, TX, 2010), Springer, to appear.
17. G. Kutyniok and W.-Q Lim, *Compactly supported shearlets are optimally sparse*, J. Approx. Theory, to appear.
18. M. A. Pinsky, N. K. Stanton, P. E. Trapa, *Fourier series of radial functions in several variables*, J. Funct. Anal. **116** (1993), 111–132.
19. E. M. Stein, G. Weiss, *Introduction to Fourier analysis on Euclidean spaces*, Princeton University Press, Princeton, N.J., 1971.